Y. Y. Zuo and A. W. Neumann

Pulmonary Surfactant and its *in vitro* Assessment Using Axisymmetric Drop Shape Analysis (ADSA): A Review

Recent progress in the study of pulmonary surfactant is reviewed. The first half of this paper provides general background in both physiological and clinical perspectives. The second half focuses on the *in vitro* assessment of pulmonary surfactant using methods based on a drop shape technique, Axisymmetric Drop Shape Analysis (ADSA). Theories, experiments, and techniques of image analysis used in these ADSA methods are briefly described. Typical applications of these methods are discussed in detail. It is concluded that the accuracy, versatility, and simplicity of these ADSA methods render them suitable to the study of pulmonary surfactant.

Key words: Pulmonary surfactant, Axisymmetric Drop Shape Analysis (ADSA), surface tension, drop shape method, image analysis

Lungentensid und seine in-vitro Bewertung mit axialsymmetrischer DropShape Analyse (ADSA): Ein Übersichtsartikel. In diesem Übersichtsartikel werden die neusten Fortschritte der Studien über Lungentenside vorgestellt. Im ersten Teil dieser Arbeit wird ein allgemeiner Hintergrund aus der physiologischen und klinischen Perspektive gegeben. Der zweite Teil konzentriert sich auf die in-vitro Bewertung von Lungentensid, die auf Methoden der axialsymmetrischen Drop Shape Analyse (ADSA) basieren. Die Theorien, Experimente und Techniken der Bildanalyse dieser ADSA-Methoden werden kurz beschrieben und typische Anwendungen im Detail besprochen. Man kann folgern, dass die ADSA-Methoden aufgrund ihrer Genauigkeit, vielseitigen Verwendbarkeit und Einfachheit für Studien über Lungentenside geeignet sind.

Stichwörter: Lungentensid, axialsymmetrische DropShape Analyse (ADSA), Oberflächenspannung, DropShape-Methode, Bildanalyse

List of Abbreviations

ADSA	Axisymmetric drop shape analysis
ALFI-S	Axisymmetric liquid fluid interface – smoothing
ALI	Acute lung injury
AFM	Atomic force microscopy
ARDS	Acute respiratory distress syndrome
BAM	Brewster angle microscopy
BLES	Bovine lipid extract surfactant
CB	Captive bubble
CBS	Captive bubble surfactometer
CCD	Charge coupled device
CED	Canny edge detector
CR	Compression ratio
CSD	Constrained sessile drop
DMPC	Dimyristoyl phosphatidylcholine
DPPC	Dipalmitoyl phosphatidylcholine
FDA	The United States Food and Drug Administration
FOPF	Fifth order polynomial fitting
FRC	Functional residual capacity
LC	Liquid-condensed
LPC	Lysophosphatidylcholine
LWB	Langmuir-Wilhelmy balance
MW	Molecular weight
PBS	Pulsating bubble surfactometer
PC	Phosphatidylcholine
PD	Pendant drop
PE	Phosphatidylethanolamine
PEEP	Positive end-expiratory pressure
PEG	Polyethylene glycol
PG	Phosphatidylglycerol
PI	Phosphatidylinositol
POPC	Palmitoyl-oleoyl phosphatidylcholine
PPoPC	Palmitoyl-palmitoleoyl phosphatidylcholine
PS	Phosphatidylserine
PVP	Polyvinypyrrolidone
RDS/nRDS	(neonatal) Respiratory distress syndrome
SA	Surface tension vs. relative area
SBT	Spinning bubble tensiometry
SED	Sobel edge detector
SFM	Scanning force microscopy
SP-A, B, C, D	Surfactant associated proteins A, B, C and D
SPH	Sphingomyelin
VAST	Volume – area – surface tension vs. time

1 Introduction

In mammalian lungs the entire alveolar surface is lined with a thin fluid continuum, called alveolar lining layer [1, 2]. It consists of an aqueous hypophase covered by a film of pulmonary surfactant [3]. The main function of this pulmonary surfactant film is to reduce the surface tension of the alveolar surface [4, 5]. This surface tension lowering ability of pulmonary surfactant plays an important role in maintaining the normal mechanics of respiration. By lowering alveolar surface tension, first, the amount of energy required to inflate the lungs is reduced by increasing pulmonary compliance (i. e. the ratio of lung volume change to an applied distending pressure); second, the likelihood of lung collapse during expiration is reduced by decreasing elastic recoil [6]. As a result, the lungs can easily maintain patency by a small transpulmonary pressure, i. e. 1 to 10 cm H_2O [7].

Deficiency or dysfunction of lung surfactant leads to severe pulmonary diseases. Neonatal Respiratory Distress Syndrome (nRDS), or simply called RDS, is the major disease of lung surfactant deficiency worldwide due to prematurity [8]. Patients with RDS are premature infants who exhibit increased work of breathing, decreased lung compliance, prominent atelectasis with reduced function residual capacity

(FRC, i. e. the volume remained in the lungs at the end of expiration), impaired gas exchange, and diffuse interstitial edema [8]. As many as 50 000 to 60 000 premature infants in the United States alone are threatened by RDS annually [8].

An adult version of RDS is Acute Respiratory Distress Syndrome (ARDS), a severe form of acute lung injury (ALI) [9]. Patients with ARDS can be of any age but exhibit similar symptoms to RDS [9]. The pathogenesis of ARDS is not fully understood but surfactant dysfunction or inactivation by a variety of inhibitory substances, such as blood, plasma and serum proteins, and meconium [10] is believed to be an operative cause accompanied with the other primary pathologies, e. g. oxygen toxicity, severe pulmonary infections, or radiation damage [11].

Exogenous surfactant replacement therapy, in which either synthetic or natural lung surfactants extracted from mammalian lungs are delivered to the patients, has been used as a standard therapeutic intervention for patients with RDS [12]. The surfactant therapy also shows favorable effect on ARDS [9].

Therefore, the study of lung surfactant has not only physiological but also clinical significance. A number of *in vivo*, *in situ* and *in vitro* methods have been developed for assessing lung surfactant as outlined later in this review. Among these methods, Axisymmetric Drop Shape Analysis (ADSA) shows an intriguing potential for *in vitro* assessment of lung surfactant.

ADSA is a surface tension measurement methodology initiated in the author's laboratory in the 1980s [13]. It has been continuously improved in the last two decades [14–18]. ADSA is found to be particularly suitable for the study of lung surfactant as it requires only a small amount of liquid sample, is capable of measuring dynamic [19] and ultralow surface tensions [20], and more importantly, is able to be operated like a microfilm balance [21].

This paper reviews the applications of ADSA in the study of lung surfactant. It is organized as follows: in Section 2, we introduce the lung surfactant system, including its composition, physiological functionality, and metabolism. Section 3 reviews the history of discovering lung surfactant and its clinical applications. Section 4 summarizes the commonly used methods for assessing lung surfactant. Focus is on *in vitro* techniques. Section 5 focuses on the description of ADSA related methods. Several typical applications are discussed in Section 6. Finally, a brief summary and some perspectives are given in Section 7.

It should be noted that the study of lung surfactant experienced a booming development in the last several decades and continues blossoming. A large body of literatures is available on physiological, biochemical, biomedical, and biomechanical aspects. It is not attempted here to cover all these aspects; rather, the focus is on the *in vitro* surface tension assessment. However, other topics, such as the surfactant composition, which are closely related to the surface tension properties of lung surfactant, are also discussed, although not in detail. The aim is to provide useful references for further reading.

2 Lung surfactant

2.1 Composition of lung surfactant

Comparative biology studies suggest that lung surfactant exists in all vertebrates, although with different compositions [22]. In mammalian lungs, however, the composition of lung surfactant is remarkably similar among diverse species, i. e. approximately 90 % lipids and 10 % proteins by weight [23].

The lipids consist of a majority of phospholipids (~97 wt %) and a small amount of neutral lipids (~3 wt %), primarily cholesterol [24]. Among the phospholipid components, phosphatidylcholine (PC), also known as lecithin, is the most prevalent class, accounting for approximately 80 wt % of the total lung surfactant phospholipids [25]. About half of PC is dipalmitoyl phosphatidylcholine (DPPC) [25]. DPPC is the most abundant single component in lung surfactant, accounting for approximately one third of the total phospholipids. DPPC is a long-chain, disaturated phospholipid (i. e. neither fatty acid chain contains a double bond.). In contrast, the other PC components are mainly unsaturated (i. e. fatty acid chains of the phospholipid contain at least one double bond) [8], e. g. palmitoyl-palmitoleoyl-PC (PPoPC) and palmitoyl-oleoyl-PC (POPC).

Apart from PC, other classes of phospholipids constitute the rest 20 wt % of the lung surfactant phospholipids. They are mainly unsaturated, including both anionic phospholipids (e. g. phosphatidylglycerol (PG), phosphatidylinositol (PI), phosphatidylserine (PS)) and zwitterionic phospholipids (e. g. phosphatidylethanolamine (PE), sphingomyelin (SPH)). Anionic phospholipids as a group account for about 12–15 wt % of the total phospholipids [25].

There are at least four known lung surfactant associated proteins, named SP-A, -B -C and -D based on the nomenclature proposed by Possmayer in 1988 [26]. SP-A (MW 26–38 kDa) and SP-D (39–46 kDa) are large hydrophilic molecules. They are members of the Ca^{2+}-dependent carbohydrate-binding collection family. In contrast, SP-B (MW 8.5–9 kDa) and SP-C (3.5–4.2 kDa) are smaller and extremely hydrophobic. Among these surfactant associated proteins, SP-A is the most abundant one, accounting for about 5 wt % of lung surfactant, followed by SP-D, accounting for about 3.5 wt %. SP-B and SP-C together constitute approximately 1.5 wt % [8].

2.2 Physiological function of lung surfactant components

At least three physical properties of a lung surfactant system are essential to the normal lung function, especially in the neonatal period [25, 27]. They are: 1) rapid film formation (i. e. within seconds) *via* adsorption from the alveolar hypophase; 2) low film compressibility (i. e. < 0.01 m mN^{-1}) associated with very low surface tension values (i. e. near-zero values) during lung deflation; and 3) effective replenishment of the lung surfactant film during lung inflation. The composition of the lung surfactant serves to fulfill these basic physiological functions.

Surface properties of phospholipids, such as surface activity, fluidity, and phase behavior, are crucially dependent on the length and saturation of their fatty acid chains [8]. The lung surfactant film at the alveolar surface must consists of a significant amount of rigid saturated phospholipids because only these phospholipids are able to be tightly packed upon lateral compression and therefore yield near-zero surface tensions [8].

First, the phospholipids must be saturated. Unsaturated phospholipids only allow a limited compression beyond equilibrium. The equilibrium surface tension is the lowest surface tension that pure or mixed phospholipid films can achieve by spontaneously spreading or adsorption [25]. Given sufficient amounts of lipid and a long enough time, identical equilibrium surface tension values for different preparations of lung surfactant are found to be in the range of 22–25 mJ m^{-2}, no matter how the film is formed [25].

Further decrease in surface tension beyond the equilibrium value can only be achieved by film compression [27]. However, for unsaturated phospholipids, the minimum surface tensions that can be reached by compression merely range from 15 to 20 mJ m^{-2} [25]. The surface tensions remain constant during further compression, indicating expulsion of phospholipid molecules out of the film, i. e. "film collapse" [25].

Second, the phospholipids must be rigid. In other words, the phospholipids should be in a gel phase at the normal physiological temperature (i. e. 37 °C). At a certain critical temperature (T_c), a hydrated phospholipid undergoes a thermotropic phase transition, called gel to liquid crystal phase transition, in which fatty acid chains of the phospholipid are "melted" and the two dimensional molecular motion is greatly enhanced [25]. After that, the phospholipid changes from a rigid, ordered, gel phase to a rather mobile, disordered, liquid-crystalline phase. T_c increases with chain length but decreases with the number of double bonds [8]. The introduction of double bonds has the most profound impact on T_c. Unsaturated phospholipids usually have a T_c far less than the body temperature (e. g. POPC has a T_c of –5 to 4 °C [8]). Under normal physiological conditions, unsaturated phospholipids are all in the liquid crystal phase and therefore form films with expanded molecular packing, easily collapsing at a low film pressure. The length of the fatty acid chains also affects T_c, albeit to a lesser extent than saturation (i. e. number of double bones) [8]. For instance, a disaturated PC with chain length of 14 carbon atoms, dimyristoyl phosphatidylcholine (DMPC) has a T_c of only 27 °C [8]. Consequently, at 37 °C, DMPC is also unable to decrease surface tension to near-zero values even though it does yield tighter packing and more condensed films than unsaturated phospholipids do [8]. Further study suggests that only disaturated PC with chain lengths of at least 16 carbon atoms are in the rigid gel phase at the normal body temperature [8].

DPPC satisfies these two requirements. DPPC is a long-chain disaturated phospholipid with a transition temperature of about 41 °C [8]. Therefore, at the normal body temperature, DPPC exhibits high rigidity and hence facilitates the formation of highly ordered, tightly packed, solid surface films, which are capable of reaching near-zero surface tensions upon compression. According to the knowledge to date, DPPC is the only component in lung surfactant responsible for such extremely low surface tensions [8].

The rigidity of DPPC at the body temperature renders it capable of reducing surface tensions to extremely low values, but also causes its poor performance in adsorption and respreading at the air-liquid interface [8]. The unsatisfactory adsorption properties of DPPC are compensated for by the presence of the unsaturated phospholipids, neutral lipids, and surfactant associated proteins [29–31]. These lipids, mainly unsaturated, are in a fluid liquid crystal phase at the body temperature and hence have a major impact in improving mobility of DPPC and enhance its adsorption and respreading at the air-liquid interface. With the aid of these fluid lipid components and the surfactant associated proteins (discussed below), lung surfactant is able to adsorb rapidly at the alveolar surface, a primary physiological necessity. After the *de novo* adsorption, the fluid phosphilipid components, which are less effective in lowering surface tensions, are squeezed out of the film during the subsequent compression, thus resulting in a condensed, DPPC enriched film [32]. As indicated before, this DPPC enriched film is responsible for the reduction of surface tensions to near-zero values.

Surfactant apoproteins also play an important role in the film formation, film refining, film stabilization at high surface pressures, and film replenishment after collapse.

SP-A shows a variety of physiological functions involving the enhancement of surface activity of lung surfactant and the maintenance of surfactant homeostasis [33]. However, SP-A alone has little effect on the surface activity of lung surfactant [34, 35] but needs to be incorporated with the hydrophobic apoproteins (e. g. SP-B) and calcium ions [34, 36, 37]. Under certain circumstances, e. g. reduced phospholipid concentrations [38–40] occurring in the impaired lungs, SP-A can significantly improve the surface activity by enhancing phospholipid adsorption and refining the surfactant film by excluding non-DPPC lipids [34, 40]. As a result, the addition of SP-A to lung surfactant extracts *in vitro* exhibits limited surface tension-area hysteresis, less compression to reach low surface tensions and increased stability [40]. SP-A is also able to resist the inhibition due to a number of substances, such as blood proteins [37, 39], cholesterol [36], and meconium [41]. Other known functions of SP-A are the formation of tubular myelin [42], maintenance of large surfactant aggregates [43], regulation of uptake and secretion of surfactant by type II cells [44] and host defense as outlined in Ref. [45, 46].

SP-B and SP-C independently promote rapid adsorption of phospholipids to the air-liquid interface [32]. They also play a role in the film refining, that is, in the selective squeeze-out of non-DPPC molecules from the interface [47–50]. In addition, SP-B and SP-C are important in the film renewal since they remain in the excluded phase on compression and enhance readsorption and respreading of the surface active compounds on expansion [47–50].

So far, no significant physiological functions regarding surface properties have been found to be associated with SP-D [45]. However, recent studies suggested that SP-D appears to be of importance in the pulmonary host defense system [51].

Detailed descriptions of the biochemical compositions of lung surfactant and their physiological functions are available in a number of excellent reviews [8, 23–25, 29–32, 52–59].

2.3 Metabolism of lung surfactant

Metabolism of lung surfactant takes place in the aqueous hypophase of the alveolar lining layer [32]. By using transmission electron microscopy, Weibel and his colleagues [3, 60, 61] convincingly demonstrated that alveoli are lined with a thin liquid layer that covers a substantial area of alveoli. The continuity of this lining layer was also established by a study of rat lungs using low-temperature electron microscopy [62]. It was found that the aqueous hypophase has an average thickness of 0.14 μm over the alveoli surface, 0.89 μm in alveolar corners, and an area-weighted average thickness of 0.2 μm [62]. Even though very thin, this hypophase is still large enough to qualify as a bulk phase compared to the surfactant film covering it, which is in the molecular dimension, i. e. nanometer range [63]. The aqueous hypophase is believed to be essential for the lung surfactant metabolism by providing a medium for surfactant secretion, transformation, adsorption, desorption, and replenishment [8].

Lung surfactant is synthesized by type II epithelial cells, and processed and packed into lamellar bodies in a structure of closely packed multiple bilayers [32]. Subsequently, lung surfactant is secreted into the alveolar hypophase, in which some of the lamellar bodies undergo transformation into an

unusual morphological form called tubular myelin [32]. Tubular myelin is composed of large cylindrical tubes constituted primarily of phospholipids and proteins, ranging in size from nanometers to microns. Tubular myelin is highly surface active, phospholipid-rich, most likely representing an immediate precursor of the lung surfactant film at the air-water interface of alveoli. From the traditional point of view, the lung surfactant film is monomolecular thick [64, 65]. However, recently, cumulating evidence, achieved by using electron microscopy [66, 67], captive bubble surfactometer [68, 69], and direct film imaging using scanning force microscopy [70], suggested that this film is most likely thicker than a monolayer.

After *de novo* adsorption, the lung surfactant film undergoes refining during the subsequent film compression and expansion, corresponding to the deflation and inflation of the lungs. On compression, the surfactant film becomes enriched in DPPC by selective squeeze-out of the non-DPPC components [32] (Alternatively, the enrichment in DPPC might be due to "selective adsorption", i. e. the film may be enriched in DPPC during the *de novo* adsorption process [71]). If the surfactant film is compressed beyond the collapse pressure, it may lose surface active material by forming three dimensional collapse phase in the subphase or forming extended multilayered structures adjacent to the film [72]. Upon the subsequent expansion, with the aid of surfactant apoproteins, the film can be effectively restored by readsorption and respreading of surface active material from the hypophase, from the so-called "surfactant reservoir" associated with the surface formed after the *de novo* adsorption, or from the collapse phase [73].

After performing their physiological function, the surfactant molecules are eventually removed from the interface and are cleaned from the alveolar space or re-uptaken by endocytosis back into type II cells, where surfactant components are recycled to reduce the need for *de novo* synthesis [32]. The turnover period of lung surfactant ranges from 4 to 11 hours [74, 75].

Other reviews on the metabolism of lung surfactant can be found in Ref. [76, 77].

3 Discovery of lung surfactant

3.1 Surface tension of lung surfactant

The discovery of lung surfactant can be traced back to 1929 when von Neergaard first introduced the importance of interfacial forces for lung mechanics [78]. By comparing the recoil pressure of lungs filled with air and with aqueous solution, von Neergaard demonstrated the existence of alveolar surface tension. However, he was not able to find a surface active material from the lungs. He also measured the surface tensions of tissue extracts and of liquid used to distend the lungs from the pressure-volume behavior. The surface tensions measured by him ranged from 35 to 41 mJ m^{-2}.

von Neergaard's study caused little attention until Pattle, in 1955, published his classic paper in *Nature* [79]. By studying the stability of microbubbles (40~50 μm in diameter) in the lung extracts, Pattle drew the conclusion that surface tensions of lung extracts should be zero. Otherwise the microbubbles could no be stabilized but would dissolve rapidly due to their internal excess pressure generated by the highly curved surface based on the Laplace equation. He concluded, erroneously, that the film responsible for the zero surface tension is composed of an insoluble protein. Pattle corrected his mistake later by identifying the film is composed of a lecithin-protein complex [80].

In 1957, Mead and his colleagues studied the dependence of lung compliance on surface tension forces [81]. They observed that, during slow deep breaths, the quasi-static transpulmonary pressure during inflation with gas was higher than that during deflation, a phenomenon called pressure-volume hysteresis. The hysteresis largely disappeared during inflation with liquid. They attributed this difference to the operation of surface tension.

In 1957, Clements performed the first direct surface tension measurement of lung extract by using a modified Langmuir-Wilhelmy balance [82]. He found that 1) the lung extracts are able to lower the surface tension to a value as small as 10 mJ m^{-2}; and 2) the surface tension-area curves of lung extracts exhibit significant hysteresis, similar to those observed in pressure-volume curves [81]. These *in vitro* surface tension properties of lung surfactant, i. e. its ability to reach low surface tension (near-zero value) and to vary surface tension during film oscillation (between approximately 30 mJ m^{-2} and near-zero values), were later confirmed by Schürch et al through direct surface tension measurement in the lungs [83].

Excellent further and detailed reviews are available [84, 85].

3.2 Lung surfactant in clinical applications

The clinical relevance of lung surfactant and RDS was first established by Avery and Mead [86]. In 1959, Avery and Mead reported that they could not find surfactant in the lung extracts of infants who died of hyaline membrane disease, later referred to as RDS, but that it was found in infants who died without pulmonary diseases, provided that their birth weight was more than about 1000 gram. Therefore, they hypothesized that prematurity and lack of surfactant were responsible for RDS. The pathological relationship between prematurity and surfactant deficiency was later confirmed by Brumley et al who found that the lung surfactant system does not mature until late in gestation [87].

The idea of treating RDS by supplying surfactant substitute to the surfactant deficient lungs has been appreciated soon after the work by Avery and Mead [86]. However, the selection of a suitable surfactant replacement remained unsolved for a long time. Shortly after DPPC was found to be the primary component responsible for surface tension decrease [88], attempts were made to treat RDS by administering aerosols of DPPC [89]. However, these early trials failed, mainly due to the poor adsorption of pure DPPC, which is far less than required by normal lungs [90]. Not until 1980, Fujiwara et al reported the first successful trial of surfactant replacement in infants with RDS by using a surfactant preparation extracted from bovine lungs [91]. At present, surfactant replacement therapy has become a standard therapeutic intervention for patients with RDS [12]. Owing to this therapy, the mortality rate of premature infants in the United States due to RDS dropped by 24 % between 1989 and 1990 and continues decreasing thereafter [92, 93].

In 1967, Ashbaugh and his colleagues first described a syndrome of acute respiratory distress in adults which closely simulates the symptoms of RDS in premature infants [94]. These workers termed it adult respiratory distress syndrome (ARDS) [95], which was later renamed acute respiratory distress syndrome. Inspired by the symptomatic similarity between ARDS and RDS, surfactant replacement therapy has been tested in ARDS [96]. It was found that surfactant therapy generally shows a positive effect on ARDS [97]. However, the effect is sometimes erratic and largely dependent on the dosage, administration, timing and the actual preparation [98].

Excellent reviews on the history and current status of surfactant therapy can be found in Ref [9, 97–103].

4 Methods to assess lung surfactants

Methods for assessing lung surfactant fall into three categories, i. e. *in vivo*, *in situ* and *in vitro* techniques.

The *in vivo* methods are usually used to test the efficacy of surfactant replacement by directly monitoring the basic physiological parameters, such as the blood oxygenation and positive end-expiratory pressure (PEEP), which are essential to evaluate the recovery of the respiratory system of animals after ALI [104]. The commonly used animal models can be generally divided into those primarily involving surfactant deficiency (i. e. surfactant-deficient newborn animals) [105, 106] and those primarily involving surfactant dysfunction or inactivation (i. e. meconium aspiration adult animals) [105, 107]. Using these *in vivo* methods, first-hand knowledge about the influencing factors of the surfactant therapy, such as efficacy of different surfactant preparations, means of administration and timing, can be gained.

The *in situ* methods refer to the methods of studying the alveolar surface tensions of excised lungs. There are two commonly used *in situ* methods allowing measurement of alveolar surface tensions. One is the microdroplet method developed by Schürch et al [83, 108–110]. By depositing droplets of test fluid (e. g. fluorocarbon) with known surface tensions onto the alveolar surface using a micropipette, these workers were able to determine the alveolar surface tension directly by monitoring the shape of the droplet during various phases of the ventilatory cycle performed in a quasi-static fashion. Another method is the pressure-volume (P-V) method initiated by Fisher et al [111], Bachofen et al [112, 113] and Wilson [114, 115] and, in which the alveolar surface tension is indirectly determined by analyzing the pressure-volume curves of excised lungs cycled in a quasi-static manner. The principle of this method is as follows: inflating or maintaining the lungs at fixed volume with air requires work against two kinds of forces, i. e. the tissue force and the surface tension force. Saline annihilates liquid-air interface that generates surface tension forces, thus leaving only lung tissue forces. The difference between P-V curves for air and saline hence reflects the contribution of surface tension forces to pulmonary mechanics. A variety of thermodynamic models have been developed to describe the correlations between the pulmonary surface tension-area behavior and the quasi-static P-V curves. For example, Prokop and Neumann [116] developed a thermodynamic model allowing for the evaluation of the alveolar surface tension, surface area, distortion energy and the mechanical work from the P-V curves of fluid- and air- filled lungs. The only assumption made in this model is that the mechanical cycling should be isothermal and quasi-static.

The *in vitro* methods examine the surface activity of natural lung surfactant extracts and therapeutic surfactant preparations. A variety of techniques have been developed for this purpose. Three widely used methods are the Langmuir-Wilhelmy balance, the pulsating bubble surfactometer, and the captive bubble surfactometer, as outlined as follows. Other reviews of these *in vitro* methods are also available [8, 27, 117–119].

4.1 Langmuir-Wilhelmy balance

The classic Langmuir balance was introduced to surface science in the early years of the 20th century [120]. Insoluble films of surfactant are formed on top of a liquid subphase contained in a trough. The film is confined by two barriers, a fixed one on the one side and an adjustable one on the other side. The film can be slowly compressed and expanded in a quasi-static fashion by moving the adjustable barrier relative to the fixed one. The force acting on the floating barrier is measured by a horizontal force transducer, which directly indicates the film pressure. Clements and his colleagues [82, 121, 122] modified Langmuir's original design and introduced the Langmuir-Wilhelmy balance (LWB) to the study of lung surfactant. In the LWB, the lung surfactant film, formed on an aqueous subphase by either spreading or adsorption, is confined in a Teflon trough equipped with a continuous Teflon ribbon border and a tightly fitted movable barrier [122]. The surface tensions are continuously monitored by a platinum Wilhelmy dipping plate. The film pressure, p, is measured indirectly, from yielding the surface tension (γ) of the film covered liquid:

$$\pi = \gamma_0 - \gamma \tag{1}$$

where, γ_0 is the surface tension of the pure liquid subphase. Not only was it an early apparatus in lung surfactant study, the LWB remains popular even now [123]. The LWB is well suited for examining surface tension-area characteristics of lung surfactant films, and particularly useful for the study of spreading films as the surface area per molecule can be accurately estimated by controlling the amount of molecules and surface area allowed for spreading. The LWB is also easy to use in conjunction with a number of film imaging apparatus, such as Brewster angle microscopy (BAM) [124–127] and fluorescent microscopy [124–130], yielding detailed structural information, e. g. the behavior of phase transition [125, 126, 130]. Companying with the Langmuir-Blodgett technique, the LWB can be also used with scanning force microscopy (SFM) [128, 131, 132] and atomic force microscopy (AFM) [133, 134], providing direct film visualization at the molecular level.

In spite of its merits, the LWB has a number of drawbacks. First, it requires a large amount of liquid sample, i. e. more than 50 mL. Second, with a generally slow cycling rate (i. e. 1~10 min per cycle), the LWB does not allow the study of fast compression simulating the frequency of breath (i. e. 20 cycles min^{-1}), as this creates a wave on the liquid surface. Third, it is well-known that measuring surface tension using a Wilhelmy plate requires a contact angle of zero degrees [135]. However, it is usually difficult to maintain a zero contact angle, especially upon re-expansion of the film, since phospholipid molecules tend to adsorb onto the plate during the previous compression and thus render it hydrophobic [136]. Finally, a less obvious but serious problem, the LWB can suffer from film leakage. Film leakage occurs because of a fundamental thermodynamic principle: at sufficiently low surface tensions, the surface active materials tend to spread from the air-water interface onto the solid that supports the film as this process decreases the total free energy of the system [137]. Due to the loss of film material and film spreading onto the solid surface, the measured surface tension and compression ratio can be essentially meaningless.

In the LWB, film leakage may occur at both the trough walls and the barriers, above (air-solid interfaces) and below the water level (liquid-solid interfaces). Since the surface tension of air-Teflon and water-Teflon is approximately 18 and 50 mJ m^{-2} [118], respectively, leakage is expected to occur whenever the film surface tension decrease below these threshold values. Leakage at the air-solid interfaces can be reduced by using tightly fitting barriers [121]. Continuous

Teflon ribbons or bands standing on edge can also help to reduce leakage at the barriers [122, 138]. Leakage at the liquid-solid interfaces can be reduced by a priming process which makes the Teflon wall hydrophilic below the water line. For example, Goerke and Gonzales [139] recommended treating the Teflon walls with an alcoholic solution of lanthanum chloride and long-chain saturated PC to reduce leakage. Using all these treatments, near-zero surface tensions can be achieved by reducing film area by 80–90 % [139]. However, this compression is almost three times greater than that *in situ* measurement and with significant hysteresis [82], indicating a failure of reproducing the *in situ* stability. Moreover, these preparation procedures considerably decrease the efficiency of the measurements.

4.2 Pulsating bubble surfactometer

The pulsating bubble surfactometer (PBS) was first introduced to lung surfactant studies by Enhorning in 1977 [140]. PBS consists of an air bubble formed in a disposable chamber containing only 20 μL of the test liquid. The bubble is suspended from a capillary connected to the atmosphere. Bubbles are formed by drawing air from the atmosphere through the capillary. Subsequently, the bubble is oscillated between two fixed positions, i. e. a maximum radius of 0.55 mm (0.7 μL in volume and 3.6 mm^2 in area) and a minimum radius of 0.4 mm (0.27 μL in volume and 1.8 mm^2 in area), by a pulsator with a stroke volume of 0.43 μL. In other words, the oscillation produces a maximum surface area reduction (i. e. compression ratio) of approximately 50 %. The cycling frequency usually used is 20 cycles min^{-1} (i. e. the frequency of breathing), but it can be changed from 0.02 to 80 cycles min^{-1}.

During oscillation, the maximum and minimum radii of the bubble are monitored by a microscope. The pressure gradient across the bubble is continuously measured by a pressure transducer. Since the bubble communicates with the ambient atmosphere, the pressure gradient measured by the transducer is the negative pressure in the liquid phase. The surface tensions are calculated by using the Laplace equation for a spherical interface (Eq. 2).

$$\Delta P = \frac{2\gamma}{R} \qquad (2)$$

where ΔP is the pressure gradient across the interface; γ is the surface tension; R is the bubble radius.

PBS is highly efficient. A repeatable assessment can be complete within 5 min. PBS has been widely used to examine the quality of surfactant preparations, i. e. 1) fast adsorption upon expansion, indicated by the surface tension at the maximum bubble radius; and 2) low surface tension upon compression, indicated by the surface tension at the minimum bubble radius. Other advantages of PBS outperforming LWB are the small amounts of sample required (20 μL), the simplicity of cleaning (disposable chamber), and the fast pulsating rate (20 cycles min^{-1}), allowing for direct simulation of breathing.

Nevertheless, PBS has a number of drawbacks. First, shared with LWB, film leakage is also a problem of PBS. At low surface tensions film leakage occurs at both the inner (air-solid interface) and the outer (liquid-solid interface) surfaces of the capillary. Leakage at the inner surface of the capillary can be reduced by keeping the tube dry [141]. However, leakage at the outer surface is difficult to remove. Due to film leakage, PBS is not suitable for the study of film stability at the minimum surface tension in a non-pulsating model. Second, the fixed maximum reduction on bubble area does not allow PBS to study the effect of compression ratio on the film compressibility and stability. Finally, even for the small bubble used in PBS, the assumption of spherical shape does not hold true when the surface tensions fall to values less than 1 mJ m^{-2} [142]. The effect of gravity on bubble deformation at low surface tensions and other effects such as surface dilatational viscosity have been well studied [143].

4.3 Captive bubble surfactometer

The captive bubble surfactometer (CBS) was first introduced by Schürch et al in 1989 [144]. In CBS, an air bubble (approximately 200 μL in volume and 7 mm in diameter) floats against a ceiling coated with 1 % agar gel, which ensures that the area of "contact" between the bubble and the chamber is completely hydrophilic. Consequently, the bubble is separated from the ceiling by a thin wetting film of the surrounding aqueous liquid, thus avoiding adhesion to any solid support and eliminating all potential pathways for film leakage [145].

Film formation in CBS is usually by adsorption [144, 145]. A spreading technique has also been developed to allow for the study of spreading films in CBS [146]. After film formation, the bubble can be cycled in either quasi-static or dynamic fashion by varying the pressure in the chamber. This can be done by varying pressure directly in a pressure-driven version of CBS [147] or by manually changing the chamber volume, i. e. moving the chamber against a fixed piston [145]. Cycling frequencies can be chosen from extremely slow to faster than 60 cycles min^{-1}.

Different from PBS, shape of the bubble in CBS cannot be assumed as spherical but turns out to be Laplacian. That is, the bubble shape is controlled by the mechanical balance between the surface tension force and local gravity, based on the Laplace equation of capillarity. Therefore, in turn, the surface tension can be determined from the bubble shape. Hence bubble images have to be acquired. These images are first enhanced by an image processing program and the bubble profiles are extracted by a simple thresholding method [148]. The remaining outliers are removed by manual editing. The bubble height (h) and diameter (d) are then determined from the bubble profile. Surface tension, bubble area and volume are calculated by substituting the ratio of bubble height to diameter (h/d) into three polynomial functions, respectively. The surface tension polynomial is modified from the formula derived by Malcolm and Elliott [149]. The polynomials of area and volume are regressed from the measurements of a series of sample bubbles with a wide range of h/d [148].

CBS is able to provide a leakage-proof experimental environment. Therefore it is well suited to study processes involving near-zero surface tensions upon compression, film compressibility, stability, and surface tension-area hysteresis [144, 145]. Without film leakage, near-zero surface tensions, mimicking the physiological surface tensions in the lungs, can be readily obtained by a moderate compression ratio (i. e. < 20 %) [71]. CBS is also capable of studying the stability of lung surfactant films in two different ways. Stability can be examined by compressing the film and holding the surface area constant. A stable film is able to maintain a low surface tension without returning towards equilibrium for many hours [150]. Alternatively, stability can be examined by studying "bubble clicks", i. e. a sudden decrease in bubble area associated with an increase in surface tension, which is though to be due to shedding surface active material from the bubble surface [144]. CBS is also flexible in

terms of independently varying the amount of film compression (i. e. compression ratio) and the speed of the compression (i. e. compression rate) [141]. Moreover, in conjunction with other techniques, CBS is able to manipulate a variety of lung surfactant characteristics which are not likely to be studied by those conventional *in vitro* methods, e. g. the demonstration of "surface-associated reservoir" using a subphase depletion technique [68].

Nevertheless, CBS also has some drawbacks. First, compared with PBS, CBS is time-consuming not only due to the complicated experimental protocol but also the tedious data processing. Second, for adsorbed films, the maximum concentration at which experiments can be conduced is restricted. Usually, the maximum concentration that can be studied is 1–2 mg mL^{-1} for a large chamber (i. e. 10 mm in diameter) and approximately 3 mg mL^{-1} for a small chamber (i. e. 5 mm in diameter) [67]. These restrictions on the concentration arise from optical limitations, since lung surfactant suspensions become murky and possibly opaque at higher concentrations.

4.4 Other *in vitro* methods

In addition to the above three most commonly used methods, there are other *in vitro* techniques for lung surfactant studies, albeit of lesser popularity. For instance, the assay can be conducted by examining microbubble stability [151–157]. Franses and his colleagues developed a spinning bubble tensiometry (SBT), in which the surface tension is calculated from a balance of centrifugal and surface tension forces at the gas/liquid interfaces [158]. Enhorning and Holm developed a capillary surfactometer, which is especially suitable to examine the effect of lung surfactant on the terminal conducting airways [159, 160].

5 ADSA methodologies

5.1 Introduction to ADSA methodologies

In the last decade, Neumann and his colleagues have developed a series of approaches based on the shape of drops and bubbles, called Axisymmetric Drop Shape Analysis (ADSA), to the *in vitro* assessment of lung surfactant. These methods are generally called ADSA methods, in which the surface tension is calculated by ADSA in conjunction with a variety of drop/bubble configurations, such as pendant drop, sessile drop or captive bubble. These ADSA methods are found to be particularly suited for lung surfactant studies due to several facts: First, the amount of liquid sample required in these methods is very small (e. g. as little as a few microliters for a drop method), which minimizes the cost of the experimental materials. Second, these ADSA methods allow for the measurement of dynamic surface tension. Therefore, it is possible to investigate the highly dynamic properties of lung surfactant, e. g. rapid film formation and dynamic cycling under physiological conditions. Third, these ADSA methods are capable of measuring very low surface tensions (i. e. less than 1 mJ m^{-2}), occurring in the lung surfactant systems. Finally, these ADSA methods are highly automated and hence operation of these methods is less dependent on the skill of the operator and they have the potential to generate a significant amount of data.

5.2 Theoretical: ADSA

ADSA was first introduced by Neumann and his colleagues in 1983 [13]. The original algorithm has been significantly improved by the same group [15]. Conceptually, ADSA determines surface tensions by numerical fitting the shape of experimental drops/bubbles to theoretical Laplacian profiles given by the classical Laplace equation of capillarity. The only assumptions made in ADSA are that the drops/bubbles are Laplacian and axisymmetric. Input parameters of ADSA are the local gravitational acceleration, density difference across the interface, and a number of coordinates of the drop profile. Typical output of ADSA includes surface tension, contact angle, drop/bubble superficial area and volume, and curvature of the drop/bubble at the apex. Running on either UNIX workstations or IBM compatible personal computers, ADSA features an easy-to-use interface and high processing speed (i. e. 1 to 2 seconds per image) [17]. Details related to the algorithms of ADSA can be found elsewhere [13, 15, 161].

ADSA has been applied to a variety of studies, including measurements of dynamic and ultralow surface tensions. In the laboratory of the authors', ADSA has been used to the study of adsorption of protein onto solid surfaces [162, 163], relaxation of protein films [164], interaction of protein and lipids [165–167], phase transition of DPPC films [168], and a number of other applications. ADSA has also been used worldwide by other laboratories for a variety of studies, e. g. protein adsorption [169], determination of solid surface tension [170], self-assembly of peptides [171], wettability of dental materials [172, 173], coating analysis [174], and the studies of lung surfactant [175–177]. Due to its accuracy, simplicity, and versatility, ASDA has been evaluated as a standard method for surface/interfacial tension measurements [178, 179].

5.3 Experimental setup

A general setup of ADSA is shown in Fig. 1. It consists of the lighting system, the image acquisition system, the environment control system, the liquid flow control system, and the different drop/bubble configurations.

The lighting system is composed of a light source (Model V-WLP1000, Newport Corp, Fountain Valley, CA, USA) and a diffuser made of frosted glass, which is used to provide uniform incident light. If rigorous lighting conditions are required, monochromatic filters can be used to provide monochromatic illumination instead of white light.

The image acquisition system comprises a microscope (Apozoom, Leitz Wetzlar, Germany), a CCD camera (Model 4815-5000, Cohu Co., USA), a digital video processor (Parallax Graphics, CA, USA) and a computer (Sparc Station-10, Sun Microsystems Inc., USA). The microscope is equipped with a polarizing filter that reduces the glare and enhances the contrast of the image. The digital video processor performs both frame grabbing and image digitizing. Image acquisition can be performed at a speed of up to 30 images per second. Each image is digitized to a matrix of 640×480 pixels with 256 grey levels for each pixel, where 0 represents black and 255 represents white. The acquired images are stored in the computer for further analysis by the image processing program.

The key environmental parameters to be controlled for a drop shape method are temperature and humidity. For a drop arrangement (sessile drop or pendant drop), a quartz glass cuvette (Model 100-QS, Hellma, USA) is used to separate the drop from the environment. A reservoir of distilled water is placed into the cuvette well before starting the experiment to guarantee a vapor-saturated atmosphere. The cuvette is placed in a stainless steel temperature cell (Model 100-07, Ramé-Hart, USA), where the temperature is thermostatically maintained by a water bath (Model RTE-111, Ne-

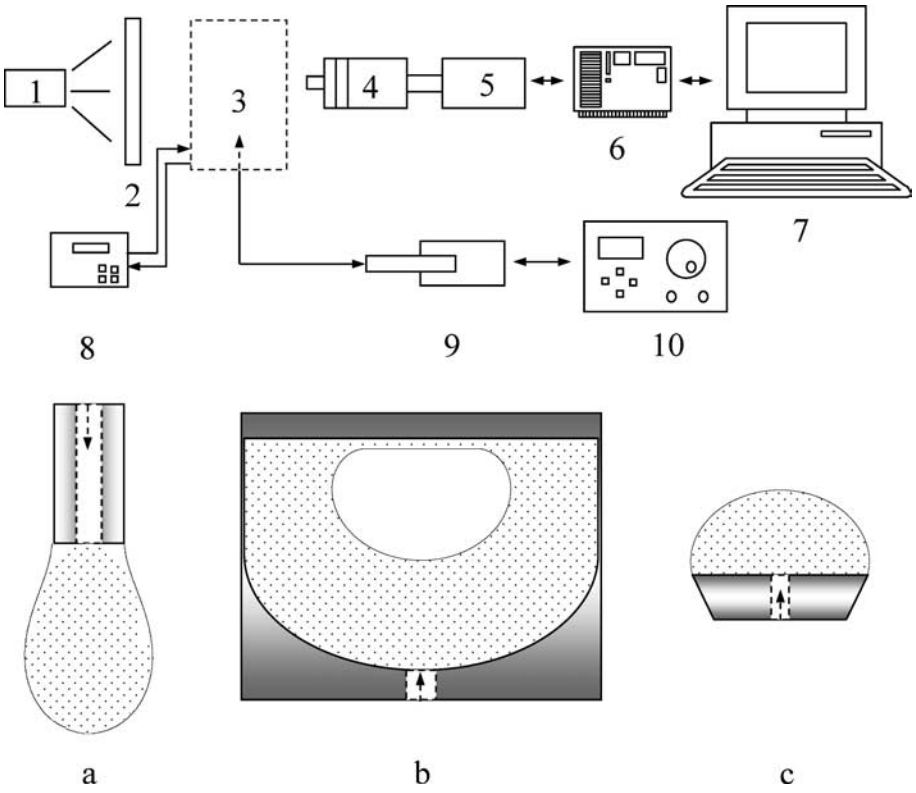

Figure 1 Schematic of the experimental set-up and three different drop/bubble configurations: (a) Pendant drop (PD); (b) Captive bubble (CB); (c) Constrained sessile drop (CSD).
1. light source; 2. diffuser; 3. thermostatic drop/bubble cell; 4. microscope; 5. CCD camera; 6. digital video processor; 7. workstation; 8. water bath; 9. motorized syringe; 10. motor controller

slab Instruments Inc, USA) within ± 0.1 °C. A Teflon stopper is used to seal the cuvette to prevent evaporation and contamination from the environment.

The control of liquid flow is necessary for the drop formation, in which a drop is initiated onto the solid support, and for the subsequent dynamic cycling, in which a drop/bubble is compressed and expanded periodically. For a drop arrangement, the flow control is performed by directly adding or withdrawing liquid into or out of the drop by means of a motor-driven syringe (Gastight, Hamilton Corp, USA). The rate and fashion of the movement of the motor, i. e. the liquid flow, is precisely controlled by a programmable motor controller (Oriel, USA). For a bubble arrangement, the motor-driven syringe is used to manipulate liquid into or out of the bubble chamber, thereby increasing or decreasing the pressure of the liquid subphase as well as in the bubble.

The entire experimental setup, except the computer, is mounted on a vibration-free table (Technical Manufacturing Corp, Peabody, MA, USA) which is equipped with compressed air bladders to minimize the effect of random vibrations. Detailed description of the ADSA hardware can be found elsewhere [180].

5.4 Different drop/bubble configurations

The selection of an appropriate drop/bubble configuration depends on the purpose of the measurement and the desired accuracy. Three different drop/bubble configurations have been used in conjunction with ADSA in lung surfactant studies. They are pendant drop, captive bubble and constrained sessile drop as outlined below.

5.4.1 Pendant drop (PD)

The PD arrangement is widely used to measure surface tension in various fields. As shown in Fig. 1 (a), a drop is suspended at the end of a capillary made of Teflon or quartz. The other end of the capillary is connected to the liquid flow control system. The capillary usually has an inner diameter of 1.0 mm and an outer diameter of 3.0 mm. Volume of the drop varies from 10 to 20 μL, corresponding to a variation in the maximum diameter from 3.0 to 3.3 mm. The vertical alignment of the capillary is maintained by a metal guide tube, which is mounted onto a three-way mircomanipulator (Model MM33-3020-0230, Leica, Germany).

A problem of the conventional Teflon capillaries is that the range of well-deformed drops that can be studied by this constellation is fairly narrow [181]. As a result, the application of a PD arrangement is significantly limited since accurate surface tension measurement can only be obtained from well-deformed drops. To circumvent this problem, a special constellation has been developed in the authors' laboratory to provide an extended range of well-deformed drops. This new constellation is an inverted pedestal (similar to that shown in Fig. 1 (c), but up side down), made of stainless steel and featuring a sharp knife edge. Hydrophilicity of the pedestal allows for the formation of well-deformed drops, favorable for accurate measurements of surface tension. The sharp knife edge is able to prevent the test liquid from spreading upon the solid surface at low surface tensions, i. e. film leakage.

In addition to the apparent advantages of simplicity and flexibility, PD features a high accuracy (i. e. ± 0.01 mJ m^{-2}) [182]. However, the PD arrangements with conventional capillaries suffer from the problem of film leakage [183], also encountered in LWB and PBS. Figs. 2 (a) and (b) show two PD images at two different surface tensions. The PD shown in Fig. 2 (a) has a surface tension of 42.14 mJ m^{-2}; in contrast, the drop shown in Fig. 2 (b) has a surface tension of 16.07 mJ m^{-2}. As seen from Fig. 2 (b), the three-phase contact line, where the capillary and drop intersect, is not discernable, indicating film leakage. The onset of the leakage was found to be approximately at 17 mJ m^{-2}. This makes in-

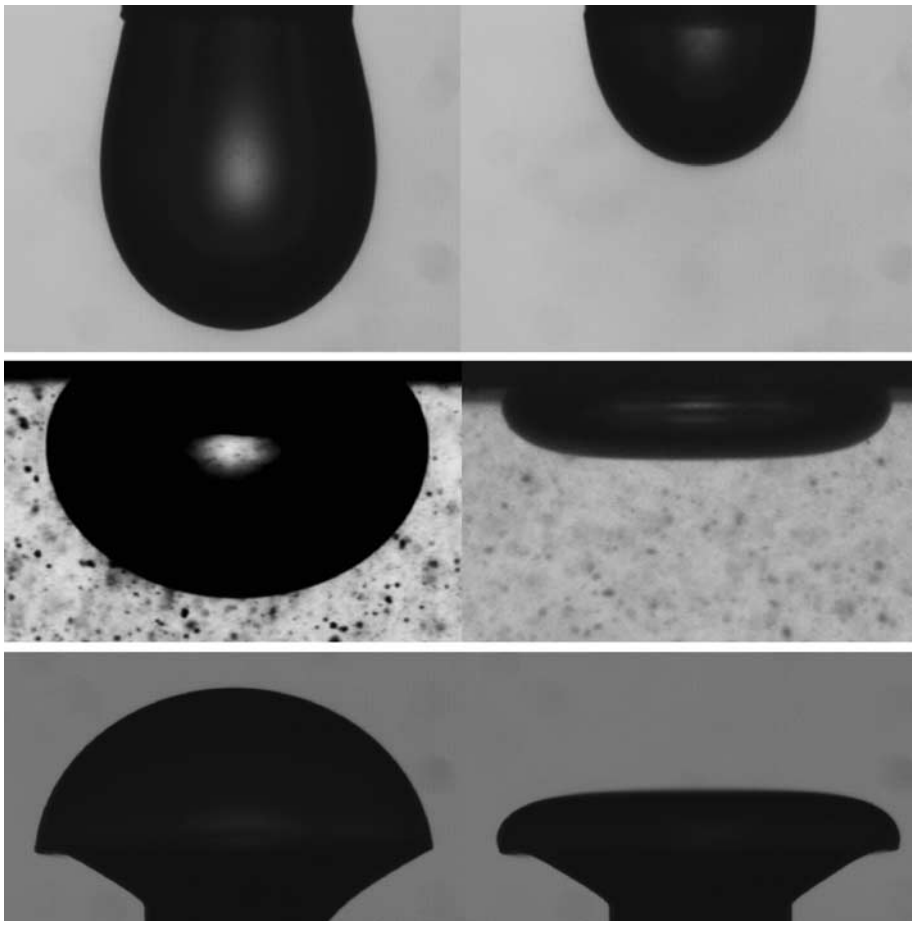

Figure 2 Images of PD, CB and CSD at different surface tensions. They are: (a) PD at 42.14 mJ/m^2; (b) PD at 16.07 mJ/m^2; (c) CB at 23.63 mJ/m^2; (d) CB at 1.25 mJ/m^2; (e) CSD at 22.56 mJ/m^2; (f) CSD at 0.42 mJ/m^2

tuitive sense from the point of view of surface energetics since the surface tension of Teflon in air is approximately 18 mJ m^{-2}. As alluded to previously, film leakage occurs when the surface tension of the film is less than that of the solid support.

Using an inverted pedestal in a PD arrangement can indeed prevent film leakage. However, another problem that may encountered at relatively low surface tensions is that the drop detaches from the constellation as under this circumstance the force of surface tension is not sufficient to balance the effect of gravity. Moreover, performance of the PD arrangement appears to be dependent on the size of the pedestal [181]. Optimal sizes for different liquids are still under investigation.

ADSA-PD was used to study the dependence of adsorption rate on the bulk concentrations of lung surfactant preparations [184] and the influence of additional nonionic polymers on the adsorption of a lung surfactant preparation [185].

5.4.2 Captive bubble (CB)

As shown in Fig. 1 (b), in a CB arrangement, a bubble with a volume of approximately 20 µL (~3 mm in diameter) is injected by a microsyringe (50 µl, Gastight, Hamilton Co., USA), into a chamber filled with a lung surfactant extract. The shape of the bubble is controlled by the surface tension. Figs. 2 (c) and (d) show two CB images at two surface tensions, 23.63 and 1.25 mJ m^{-2}, respectively. The captive bubble chamber currently used by the authors consists of three metal plates made of stainless steel and two viewing windows. Before each experiment, the chamber is assembled by sandwiching the two windows within the metal plates. The middle plate is essentially a spacer to provide a reservoir of about 1 mL. The top of the reservoir is slightly concave and serves as a "ceiling" that confines the bubble. The ceiling of the captive bubble chamber is designed to be hydrophilic. Consequently, the air bubble is separated from the ceiling by a thin wetting film, thus eliminating film leakage. The temperature and gauge pressure inside the chamber are continuously monitored by an ultrafine thermocouple (AWG40, T-type, Teflon insulated, Omega Eng Inc, Laval, Quebec, Canada) and a pressure transducer (DP15 with No. 40 diaphragm, Validyne Eng Corp, Northridge, CA, USA), respectively. A universal data acquisition card (UPC601-U, Validyne) installed in a computer is used to simultaneously process both the temperature and pressure signals.

In the authors' laboratory, ADSA-CB was used to investigate the stability of lung surfactant [186] and polymer enhanced lung surfactant films [187, 188]. It was also used to study effect of lung surfactant film on oxygen transfer [189]. In the other laboratories, Hall and his colleagues used ADSA-CB to study phase separation and transition of a lung surfactant film [175]. Pison and his colleagues [176, 177] used ADSA-CB to study the surface dilatational properties, such as surface viscosity and elasticity, of DPPC and DPPC/protein films. By spreading DPPC inside a bubble, ADSA-CB was used to study the interaction between the monolayer and the evaporated spreading solvents [190].

5.4.3 Constrained sessile drop (CSD)

CSD is a novel drop configuration for surface tension measurements. As shown in Fig. 1 (c), a sessile drop is sitting on

a pedestal, which employs a horizontal sharp-knife edge to prevent film leakage at low surface tensions. The pedestal is machined from stainless steel (SS316) with a diameter in the range of 2.5 to 4 mm. The angle between the horizontal and the side surfaces of the pedestal is in the range of 45° to 60°. The pedestal has a central hole of 0.5 mm in diameter, through which the drop is connected to the liquid flow control system by a Teflon capillary. In the experiment, a sessile drop with a volume of 4~8 μL is formed dependent on the size of the pedestal. The shape of the drop varies according to its surface tension. Figs. 2(e) and (f) show two images of CSD at surface tensions of 22.56 and 0.42 mJ m^{-2}, respectively.

No apparent limitations have been found associated with CSD. It eliminates both the problems of film leakage, as in LWB and PBS, and of concentration restriction, as in CBS. In addition, compared with the CB arrangement, CSD is much simpler and easier to operate and clean, and requires much smaller amount of test liquid (i. e. ~1 % of that used in the CB experiment).

ADSA-CSD has been used to examine the surface activity of lung surfactant at high concentrations (i. e. > 3 mg mL^{-1}) [191].

5.5 Image analysis

5.5.1 Introduction to image analysis

As indicated in Section 5.2, ADSA requires coordinates of the drop/bubble profile as input of the program. These coordinates are detected from the digital image of the drop/bubble. The accuracy of ADSA to determine the surface tension is crucially dependant on these edge coordinates [192]. Therefore, a sophisticated image analysis scheme is an indispensable part of the entire ADSA algorithm. A general image analysis scheme consists of edge detection, edge smoothing, and, if a highly accurate measurement is required, edge correction [17].

1) Edge detection
Edge detection refers to the process of detecting and locating edges of images. The edge in an image is characterized by rapid change in the optical properties, such as intensity and reflectivity [193]. The general interest in the information associated with edges provoked the development of numerous edge detectors using a variety of algorithms. Due to the inherent attribute of an edge, i. e. discontinuity in the intensity, derivative algorithms are the most popular approach to develop edge detectors [194]. Both the first and the second order derivatives are used in practice. The first order derivatives are used in those gradient algorithms, which are one of the earliest edge detection strategies. They measure the local maxima of the gradient across an edge. Pioneer gradient edge detectors include the Roberts, Prewitt, and Sobel operators [195]. The second order derivatives are usually implemented by using the Laplacian, in which the edge points are located by finding the zero-crossings of the Laplacian, e. g. the so-called LoG edge detector.

Most of these traditional edge detectors, e. g. Sobel and even LoG, are not robust against noise [196]. Promoted by the rapid development of computer science, most recent edge detectors are increasingly strong in eliminating noise. Their algorithms are based on optimal filters [197–200], fuzzy techniques [201], neural networks [202], discrete singular convolution algorithms [203], and a number of other algorithms.

Recent evaluation and comparison of different edge detection algorithms can be found in Ref. [204–206]. A number of excellent monographs, generally in image analysis, also cover the field of edge detection [193–195, 207].

2) Edge smoothing
Edge smoothing refers to the process of removing remaining noise after edge detection. It is a necessity for processing a noisy image where the edge detecting process is usually not sufficient to suppress all noise.

Two edge smoothing techniques, the fifth order polynomial fitting (FOPF) and axisymmetric liquid fluid interface – smoothing (ALFI-S), have been developed for smoothing Laplacian-akin curves [17]. Being a superior, the latter will be introduced in Section 5.5.3.

3) Edge correction
Edge correction refers to the correction of optical distortion generated by the image acquisition hardware (microscope, camera and digital video processor). Such optical distortion, e. g. the so-called pin cushion and barrel distortion, can cause major errors in the final results, particularly in the surface tension [14].

To correct the optical distortion, an image of a calibration grid pattern (square pattern with 0.25 mm spacing, Graticules Ltd., Tonbridge Kent, UK) on an optical glass is taken at the same position where the drop/bubble images are taken. Subsequently, a mapping function based on the comparison between the distorted grid image and the original grid pattern (without optical distortion) is calculated and applied to all of the drop/bubble images. The accuracy of this correction is ± 1 pixel [14]. Details about the distortion correction algorithm can be found elsewhere [14, 161].

5.5.2 Image analysis for pendant/sessile drops

As shown in Figs. 2 (a), (b), (e), and (f), images of pendant/sessile drops exhibit a distinctive edge, i. e. a dark objective (the drop) against a bright background (surroundings). For processing these drop images, the Sobel edge detector (SED) was originally invoked in ADSA [14]. The SED is a simple gradient edge operator with a small convolution mask (i. e. 3×3 pixels). The gradient of each pixel is evaluated from its neighbours within a square region of 3×3 pixels. Subsequently, the edges are determined by the pixels with the steepest grey level gradient, moving from the outside of the drop to the inside, across the interface. Detailed implementation of the SED can be found elsewhere [14, 161].

Thanks to the sharp edge of a pendant/sessile drop, the SED is usually adequate to extract an undisturbed edge from a digital image. Therefore, the edge smoothing procedure is not necessary for processing drop images.

5.5.3 Image analysis for captive bubbles

Processing captive bubble images entails an edge detector robust against noise. As shown in Figs. 2 (c) and (d), a captive bubble image is usually noisy and/or shows lack of contrast since the bubble is encompassed by a test liquid, such as lung surfactant, containing more or less insoluble phospholipid aggregates or vesicles. Therefore, the SED is not applicable because it is vulnerable to noise [196]. Thresholding is a commonly used method for processing captive bubble images [148, 183]. Nevertheless, thresholding significantly decreases the accuracy [17, 183].

Recently, the Canny edge detector (CED) has been employed in ADSA to process a captive bubble image [17, 18]. The CED [197] is an advanced edge operator based on an op-

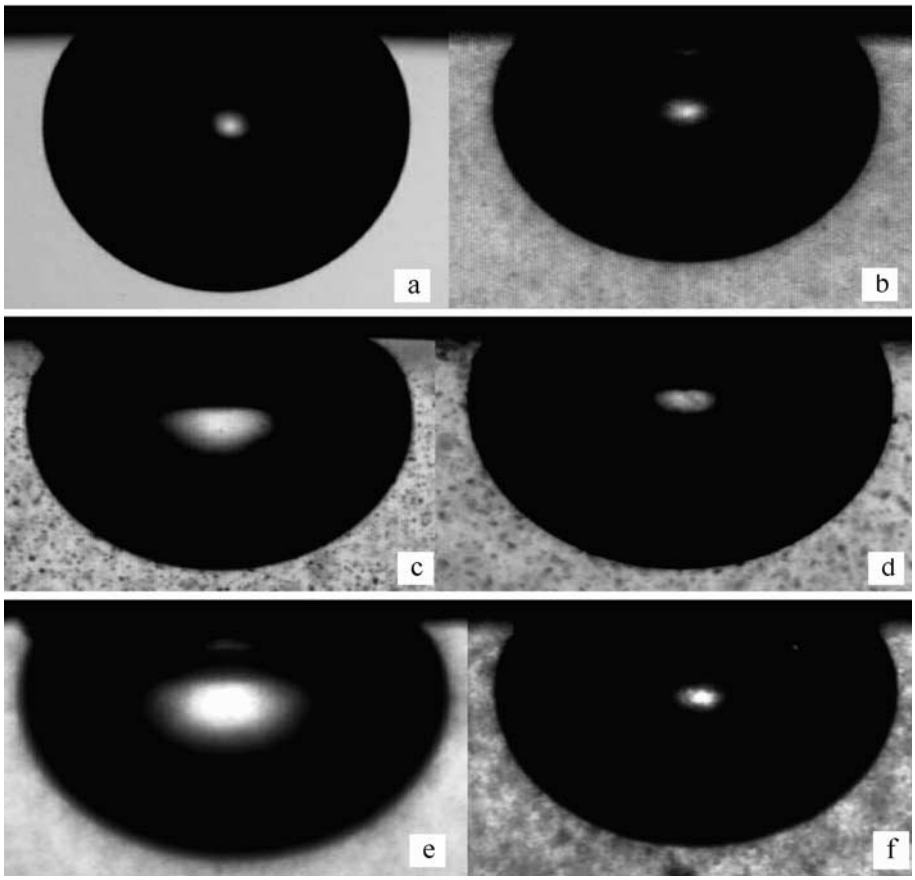

Figure 3 Six sample images of captive bubbles in different liquids. They are: (a) Distilled water; (b) 0.5 mg/ml BLES; (c) 0.5 mg/ml BLES + 30 mg/ml PEG; (d) 0.5 mg/ml natural lung surfactant; (e) 1 mg/ml BLES + 50 mg/ml PEG; (f) 0.8 mg/ml BLES + 27 mg/ml PEG

timal filter, i. e. the first derivative of a Gaussian filter. The CED is highly noise-resistant and thus very suitable for processing captive bubble images. Details implementation of the CED can be found elsewhere [17].

Edge smoothing is found to be equally important as edge detection in ADSA-CB [18]. Edge smoothing is performed in two steps. First, any detected edge point far away from the main bubble profile (i. e. isolated noise) is eliminated by measuring coherence of the adjacent points. Subsequently, those noise points attached to bubble profile (i. e. adhering noise) are removed by ALFI-S [17]. ALFI-S is a novel technique to smooth an obscured or disturbed drop/bubble profile. In ALFI-S, an experimental profile is fitted to the best matched theoretical Laplacian curve and questionable edge points that deviate from the theoretical curve are rejected as outliers. The criterion to detect and reject the outliers is 3s where s is the standard deviation evaluated from the distances between each experimental edge point and the closest theoretical point. ALFI-S is performed iteratively until no more outliers are found.

Performance of ADSA-CB was examined for six typical images of captive bubbles. As shown in Fig. 3, six images were chosen to represent a wide variety of conditions of noise and contrast. In each image, a captive bubble is resting against the ceiling and is surrounded by a certain liquid. These liquids are (a) distilled water; (b) 0.5 mg mL^{-1} BLES; (BLES is the brand name of a therapeutic lung surfactant preparation. SP-A and other components, e. g. SP-D and neutral lipids, are absent from BLES. Detailed composition of BLES is introduced later.) (c) 0.5 mg mL^{-1} BLES + 30 mg mL^{-1} polyethylene glycol (PEG); d) 0.5 mg mL^{-1} natural lung surfactant (Natural lung surfactant consists of all phospholipid and protein components, including SP-A); (e) 1.0 mg mL^{-1} BLES + 50 mg mL^{-1} PEG; (f) 0.8 mg mL^{-1} BLES + 27 mg mL^{-1} PEG. Except for the first image, which was taken at 20 °C, the others were at 37 °C. The first two images represent clean images free of noise. Figs. 3 (c) and (d) represent images with extensive noise. Noise in these two images may be due to SP-A-stabilized and PEG-induced large surfactant aggregates (see Section 6.4 for detailed discussion), respectively. Figs. 3 (e) and (f) are examples of lacking contrast due to the relatively high surfactant concentrations.

The extracted edges right after performing the Canny edge detection are shown in Fig. 4. It is noted that even though some noise points still exist, CED successfully extracts all edges. A general profile consists of about 700 to 800 edge points. For the clean images shown in Fig. 3 (a) and (b), the extracted edges are very smooth. For the noisy and low contrast images, satisfactory edges are also obtained. The broken edge shown in Fig. 4 (d) is due to the non-uniform distribution of intensity in the digital image (see Fig. 3 (d)). However, in spite of the deficiency on the left side, the right side of the edge is completely preserved. Since the bubble profile is assumed to be axisymmetric, one side of the bubble profile is adequate for ADSA calculation as long as that side is complete and accurate.

Fig. 5 shows the smoothed edges after ALFI-S. It is noted that ALFI-S is capable of yielding smooth edges for all the images under diverse conditions. And, the numbers of edge points for different bubble images are roughly the same, i. e. 700, after edge smoothing.

The surface tensions measured from the images shown in Fig. 3 are summarized in Tab. 1. Analysis of each image is performed in four different ways. They are: (1) calculation using the whole profile without optical distortion correction

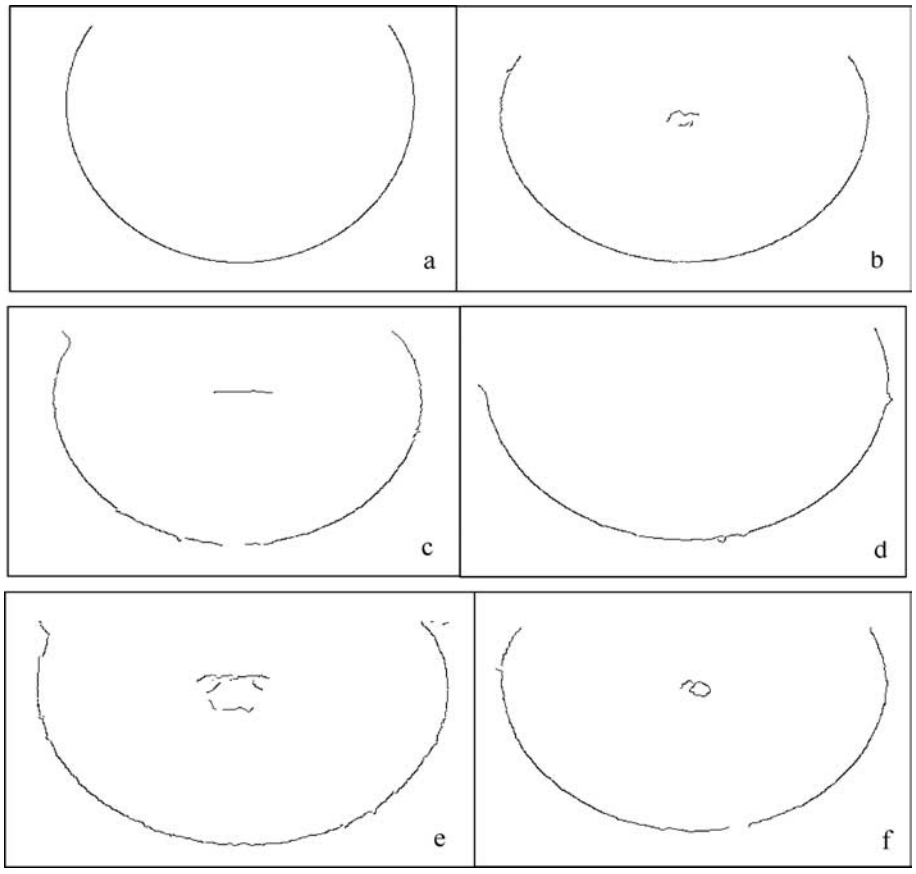

Figure 4 Extracted edges from images shown in Fig. 3 right after the Canny edge detection. The detected numbers of edge points are: (a) 776; (b) 739; (c) 705; (d) 737; (e) 826; (f) 726

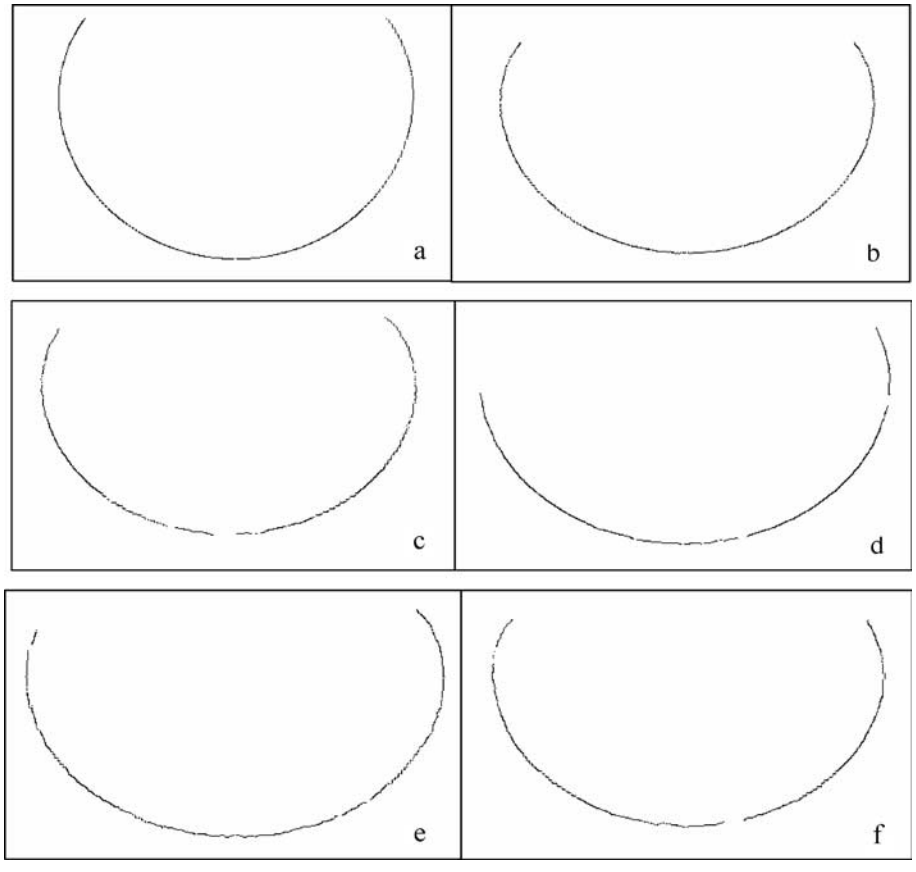

Figure 5 Smoothed edges after removing isolated noise and adhering noise using ALFI-S. The remaining numbers of edge points are: (a) 742; (b) 724; (c) 667; (d) 683; (e) 756; (f) 700

(WP – DC); (2) calculation using the whole profile with optical distortion correction (WP + DC); (3) calculation using 50 randomly selected edge points 10 times without optical distortion correction (50 × 10 – DC); (4) calculation using 50 randomly selected edge points 10 times with optical distortion correction (50 × 10 + DC). The values of surface tension calculated using randomly selected points are shown with the 95 % confidence intervals.

Also listed in Tab. 1 are the optimal user-specified parameters used in CED for the different images. To achieve optimal performance, any edge detector requires user-specified parameters *a priori*. In CED, the primary parameter is the standard deviation (σ_G) of the Gaussian filter. A straightforward procedure has been developed to determine the optimal parameters for CED [17].

Image	σ_G[1]	WP – DC[2]	WP + DC[3]	50 × 10 – DC[4]	50 × 10 + DC[5]
a	0.4	72.78	72.89	72.26 ± 1.11	73.17 ± 0.91
b	1.4	28.63	29.23	28.58 ± 0.42	29.62 ± 0.32
c	3.6	25.73	26.55	25.55 ± 0.18	26.34 ± 0.28
d	3.0	28.17	27.97	27.86 ± 0.24	27.88 ± 0.31
e	1.4	23.65	23.56	23.56 ± 0.21	23.75 ± 0.24
f	3.2	24.53	25.03	24.36 ± 0.34	24.91 ± 0.29

Results calculated using the randomly selected points are shown with 95 % confidence intervals.

1: the standard deviation of the Gaussian filter used in the CED;
2: calculation using the whole profile (WP) without optical distortion correction (DC);
3: calculation using the whole profile with optical distortion correction;
4: calculation using randomly selected 50 points 10 times without optical distortion correction;
5: calculation using randomly selected 50 points 10 times with optical distortion correction.

Table 1 Surface tensions (mJ/m^2) for images shown in Fig. 3 measured using ADSA-CB

To examine the dependence of ADSA results on this user-specified parameter, a captive bubble image in a mixture of 0.5 mg mL^{-1} BLES and 50 mg mL^{-1} PEG (as shown in Fig. 2 (c)) is analyzed by varying σ_G. The key ADSA results, i. e. surface tension, bubble area, volume and curvature of bubble at the apex, are listed in Tab. 2. It is worth noting that, on the one hand, surface tension and curvature are directly optimized from ADSA by numerical fitting the detected experimental profile to the theoretical Laplacian curves; on the other hand, the surface area and volume of a captive bubble are calculated separately by extrapolating the best matched Laplacian curve to 180°, where the bubble coincides with the wetting film separating the bubble from the ceiling. In addition, the area in contact with the wetting film is also carefully evaluated and added as part of the surface area of the bubble [18].

From Tab. 2, it is clear that over a large range of σ_G, from 1.0 to 4.0, the ADSA results are very consistent and there is no apparent dependence of ADSA results on σ_G. The 95 % confidence intervals associated with the mean values of all ADSA results are very small, indicating good reproducibility. In other words, CED is not sensitive to the selection of the user-specified parameter.

CED and ALFI-S both contribute to the high reproducibility shown in Tab. 2. The numbers for remaining and deleted edge points after ALFI-S is applied are also listed in Tab. 2. It is noted that for different values of σ_G, the num-

σ_G	Surface tension (mJ/m^2)	Area (cm^2)	Volume (cm^3)	Curvature at apex (cm^{-1})	Remaining edge points[2]	Deleted edge points[2]	ALFI-S Iteration[2]
0.8	Failed						
1.0	23.65	0.3612	0.01906	4.271	695	171	9
1.2	23.68	0.3613	0.01906	4.272	701	153	8
1.4	23.74	0.3616	0.01908	4.274	748	132	8
1.6	23.74	0.3616	0.01908	4.274	743	124	7
1.8	23.74	0.3616	0.01908	4.274	747	76	7
2.0	23.72	0.3615	0.01908	4.273	752	81	7
2.2	23.70	0.3615	0.01907	4.272	762	23	5
2.4	23.70	0.3615	0.01907	4.272	763	24	5
2.6	23.70	0.3615	0.01907	4.272	759	15	4
2.8	23.64	0.3614	0.01906	4.270	741	16	4
3.0	23.63	0.3615	0.01906	4.269	669	14	4
3.2	23.64	0.3615	0.01906	4.269	667	16	4
3.4	23.63	0.3615	0.01906	4.269	666	17	5
3.6	23.64	0.3614	0.01906	4.270	727	16	4
3.8	23.64	0.3614	0.01906	4.270	724	16	4
4.0	23.64	0.3614	0.01906	4.270	724	16	4
Mean	23.677 ± 6.69 × 10^{-4}	0.36146 ± 1.71 × 10^{-6}	0.019067 ± 1.37 × 10^{-7}	4.2713 ± 2.85 × 10^{-5}	724	57	5.6

The mean values of the ADSA-CB results are shown with 95 % confidence intervals.

1. The calculations are based on the captive bubble image shown in Fig. 2 (c) using the whole profile without correction of optical distortion.
2. The last 3 columns list the numbers of remaining and deleted edge points after ALFI-S, and the number of iterations of ALFI-S.

Table 2 ADSA-CB results[1] as a function of the user-specified parameter of CED, standard deviation of the Gaussian filter (σ_G)

bers of finally remaining edge points are similar and around 720. However, a considerably larger number of points are removed by ALFI-S when σ_G is small. Accordingly, more iterations are needed. This is due to the fact that if s_G is small, the Gaussian filter used in CED is less effective in noise suppression (but faster in the calculation), thus leaving more noise after the edge detection step [5]. In this situation the following edge smoothing step, ALFI-S, is responsible for further noise reduction, which renders the final number of edge points relatively constant. When σ_G is decreased to 0.8, too much noise remains after edge detection to be removed by ALFI-S, thereby causing the failure of ADSA.

The accuracy of ADSA-CB was examined by measuring the surface tensions of distilled water and comparison with the literature value [208, 209]. It was found that using the whole profile and correcting optical distortion, a general accuracy better than 0.1 mJ m^{-2} can be achieved [17].

6 Typical applications of ADSA methods in lung surfactant studies

Insights into the physiological function of lung surfactant, i. e. fast adsorption, low compressibility at high surface pressure, and efficient film replenishment upon film expansion, can be gained by different ADSA methods. ADSA-PD is well suitable for the study of adsorption due to two facts: 1) adsorption in a PD is very sensitive to different surfactant preparations and their concentrations [210]; hence, ADSA-PD is capable of discerning even subtle difference in the adsorption kinetics; 2) the limitation of film leakage is less pronounced in the study of adsorption since the minimum surface tensions reached are those equilibrium values (i. e. 22~25 mJ m^{-2}), which are well above the threshold below which leakage may occur. ADSA-CB is suited to the study of film compressibility and stability, especially at low surface tensions, because this constellation is able to reproduce the *in situ* alveolar environment, i. e. fast adsorption, low surface tensions yielded by moderate compressions, and extraordinary film stability [144]. Eliminating both film-leakage and optical restrictions, ADSA-CSD is very suitable for the measurement of very low surface tensions of lung surfactant films due to adsorption from the subphase at physiologically relevant phospholipid concentrations (i. e. > 3 mg mL^{-1} [211]).

Several typical applications of ADSA methods in the studies of lung surfactant are addressed as follows. The following aspects are addressed: 1) the effect of bulk concentration on the adsorption rate, 2) the effect of compression ratios on the surface tension-area isotherms; 3) the very low surface tensions at high surfactant concentrations; and 4) the enhancement of film formation by nonionic polymers.

The lung surfactant preparation used in this study is called Bovine Lipid Extract Surfactant (BLES; BLES Biochemicals Inc, London, ON, Canada). BLES is a therapeutic surfactant commercially available. BLES is prepared from bovine natural lung surfactant obtained by bronchopulmonary lavage with organic extraction. BLES contains about 98 % phospholipids (45 % DPPC, 35 % unsaturated PCs, 12 % PG, 1 % PI, 2 % PE, 1 % lysophosphatidylcholine (LPC) and 2 % SPH and 2 % proteins. The protein components in BLES are only SP-B and SP-C. High molecular weight hydrophilic proteins, SP-A and SP-D, are removed during organic extraction. BLES is stored frozen in sterilized vials with an initial concentration of 27 mg mL^{-1}. It is diluted to the desired concentration by a salt solution of 0.6 % NaCl and 1.5 mM $CaCl_2$ on the day of the experiment. The water used in the experiments is demineralized and doubly distilled.

6.1 Effect of bulk concentration on adsorption rate

Fig. 6 shows four individual measurements of adsorption of BLES at a low concentration of 0.1 mg mL^{-1}. The measurements were conducted using ADSA-PD at 37 °C. For all runs, the surface tensions decrease from a value close to that of the air-water interface (~70 mJ m^{-2}) at time-zero. The drop formation occurred within approximately 1.5 s and time-zero refers to the end of drop formation. It is noted that the decrease of surface tension is significantly enhanced by a series of random, stepwise drops occurring within a very short period (< 0.2 s). These sudden drops in surface tension are referred to as "adsorption clicks" [145]. The magnitude of adsorption clicks can be either large (e. g. approximately 35 mJ m^{-2}) or quite moderate (e. g. in a range of 1–5 mJ m^{-2}). Adsorption clicks may be due to a quick and cooperative movement of large flakes of aggregated surfactant molecules into the air-liquid interface [71]. Since the addition of these massive aggregations of surfactant molecules dramatically increases the surfactant surface concentration, surface tension abruptly drops. The fact that both

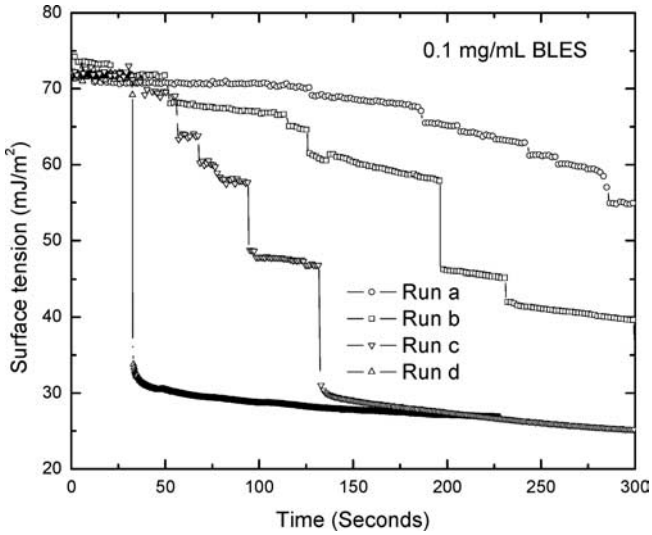

Figure 6 Adsorption of 0.1 mg/mL BLES. Surface tensions of four individual runs are plotted as a function of time. Studied using ADSA-PD at 37 °C

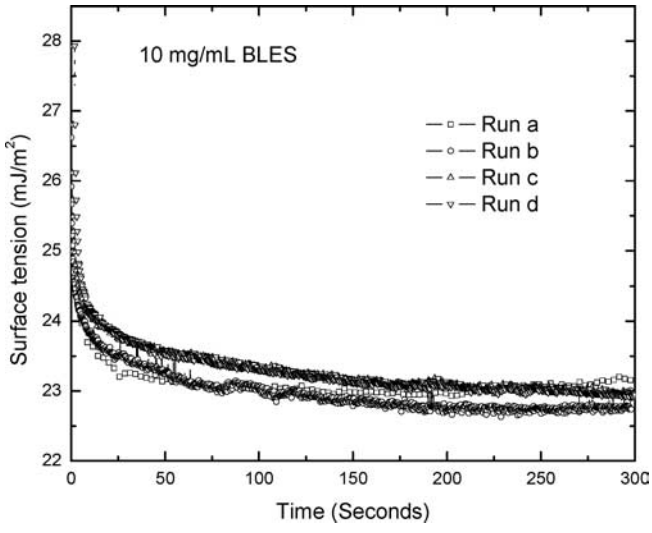

Figure 7 Adsorption of 10 mg/mL BLES. Surface tensions of four individual runs are plotted as a function of time. Studied using ADSA-PD at 37 °C

the magnitude and the occurrence of adsorption clicks are unpredictable agrees with this hypothesis. Furthermore, it is noted that significant adsorption clicks usually occur at surface tensions above 40 mJ m^{-2}. Presumably, at low surface tensions, the relatively high surface concentration of surfactant blocks further access of large aggregates to the surface and therefore impedes adsorption clicks.

Because of adsorption clicks, the surface tension kinetics obtained from individual runs is quite random. For example, in run (a) a surface tension of only approximately 55 mJ m^{-2} is reached after 300 s. On the other hand, run (d) goes well below 30 mJ m^{-2} in the first 100 s, due to a big adsorption click at about 30 s after commencing this run.

In contrast, as shown in Fig. 7, the measurements of adsorption at a high BLES concentration of 10 mg mL^{-1} are quite different from those at the low concentration (see Fig. 6). It is noted that adsorption clicks are absent. As a result, the surface tension curves measured from individual runs are consistent, i. e. the surface tensions only decrease quickly in the first 50 s, and level off in the rest 250 s. Equilibrium values in the range of 22~25 mJ m^{-2} can be reached in less than 10 s. It should also be noted that at time-zero, the surface tensions are already below 28 mJ m^{-2}. These low initial surface tensions may be due to considerable adsorption clicks occurring during the formation of the drop. However, this process is too fast to be followed by the current methodology.

Adsorptions at a variety of BLES concentrations in the range of 0.1 to 10 mg mL^{-1} were tested [184]. It was found that the adsorption clicks are not significant provided that the BLES concentration is more than 1 mg mL^{-1}. Further increasing the BLES concentration has no pronounced effect on the adsorption kinetics. Tab. 3 collects the averaged surface tensions after 2, 20 and 300 s of adsorption for BLES concentrations from 1 to 10 mg mL^{-1}. It can be seen that increasing BLES concentration from 1 to 10 mg mL^{-1} only causes approximately 1 mJ m^{-2} difference in the dynamic surface tensions.

It is concluded that the adsorption kinetics of lung surfactant depends strongly on the bulk concentration of the phospholipids. At a physiologically relevant concentration (i. e. >3 mg mL^{-1}) the formation of lung surfactant film at an air-water interface is completed within a few seconds.

6.2 Effect of compression ratio on surface tension-area isotherms

Dynamic cycling, i. e. a simulation of respiration, was studied by ADSA-CB at 37 °C. The lung surfactant film was formed by rapid adsorption (film formation completed within 5 s) from 0.5 mg mL^{-1} BLES suspension. Subsequently, the film was continuously compressed and expanded at a frequency of 12 cycle min^{-1}. The effect of the compression ratio (CR) (defined as the ratio of the maximum reduced surface area to the initial surface area) on the surface tension-relative area (SA) isotherms was investigated. Only the first five cycles were studied since the cycles afterwards are essentially identical.

BLES Concentration (mg/mL)	Surface tension (mJ/m²) (after 2 s adsorption)	Surface tension (mJ/m²) (after 20 s adsorption)	Surface tension (mJ/m²) (after 300 s adsorption)
1	26.0 ± 0.1	24.7 ± 0.1	24.0 ± 0.2
2	25.6 ± 0.1	24.7 ± 0.1	23.9 ± 0.1
3	26.0 ± 0.1	24.5 ± 0.1	23.9 ± 0.1
6	25.8 ± 0.2	24.3 ± 0.3	23.6 ± 0.2
8	25.1 ±0.1	24.0 ± 0.1	23.4 ± 0.1
10	24.9 ± 0.1	23.9 ± 0.1	22.9 ± 0.1

Each value shows as an average of four individual runs with 95 % confidence intervals.

Table 3 Surface tensions after 2 s, 20 s and 300 s of the adsorption, for a variety of BLES concentrations in the range of 1 to 10 mg/mL

Fig. 8 shows the SA isotherms at a low CR less than 20 %. Several important points should be noted. First, the CR for all five cycles, including the first one right after the *de novo* adsorption, is only 17 %. Second, the minimum surface tension reached by this small CR is less than 5 mJ m^{-2} and the maximum surface tension at the end of expansion is no more than 30 mJ m^{-2}. Third, except for the first cycle, the compression and expansion portions of these SA isotherms coincide completely, i. e. no SA hysteresis is observed. A cycle with this feature is termed as "reversible cycle" [186]. Fourth, a compression shoulder appears in the first cycle at a surface tension near 15 mJ m^{-2}. It soon disappears in the subsequent cycles. This compression shoulder may imply film refining by squeezing-out the non-DPPC materials. Finally, the compressibility

$$\mathrm{Cm} = \frac{1}{\mathrm{A}}\frac{\mathrm{dA}}{\mathrm{d}\gamma} \tag{3}$$

at the surface tension of 15 mJ m^{-2} calculated from the first compression is only 0.0070 m mN^{-1} [18]. For the subsequent four cycles Cm is slightly smaller and constant at 0.0065 m mN^{-1}. The extremely low compressibility of the first compression is close to that of a pure DPPC film, i. e. 0.005 m mN^{-1} [144]. The finding, therefore, implies that the lung surfactant film is likely enriched in DPPC right after the *de novo* rapid adsorption. In addition, Davies and Rideal [212] reported that the compressibility of a liquid condensed (LC) film is in the range of 0.004 to 0.01 m mN^{-1}. Therefore, the results apparently imply that, at a surface tension of 15 mJ m^{-2}, the lung surfactant film is predominantly in the LC phase.

Fig. 9 shows the SA isotherms at a high CR of about 60 %, which is more than three times of that used in Fig. 8. It is clear that the patterns of these isotherms are different from those at low compression ratio. First, significant hysteresis loops appear. A cycle with this feature is referred to as "irreversible cycle" [186]. Second, except for the first cycle, compression shoulders appear in these cycles at the surface tension of 20–25 mJ m^{-2}. Third, two plateaus appear at the ends of compression and expansion, in which the surface tension only slightly varies even though the bubble area changes significantly. It suggests that there are other mechanisms apart from the variation of surface area playing a role in changing the surface concentration of the lung surfactant molecules. The compression plateau occurs at a surface tension near or below 1 mJ m^{-2} (i. e. the collapse surface tension of PCs). It usually implies film collapse [71], in which the film is compressed to the point at which it can no longer support the surface pressure and hence collapses. Some surfactant molecules may transfer into the bulk liquid or form multilayer structures, causing a reduction of surfactant concentration at the interface, so that the surface tension will not decrease further. It should be also noted that there are a number of points missing in the collapse region shown in Fig. 9. This is due to the fact that film collapse causes dynamic instabilities and hence vibration of the bubble. Such vibrations cause the failure of ADSA in the col-

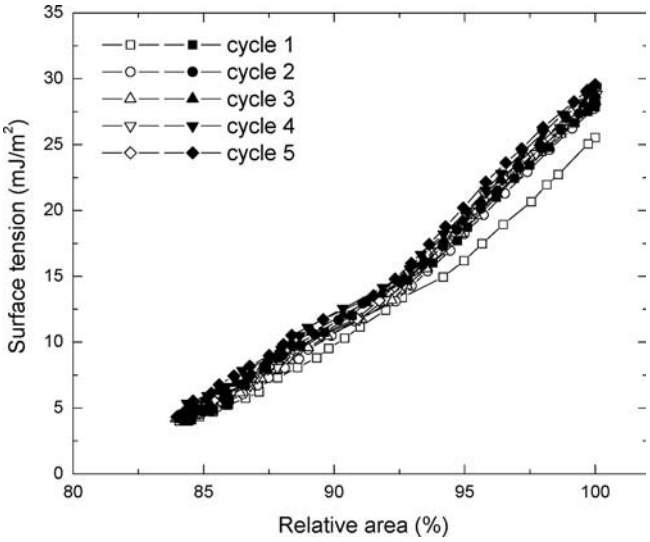

Figure 8 SA isotherms of reversible cycling, showing overlapped compression (open symbols) and expansion (solid symbols) portions in each cycle. The experiment was conducted at a low compression ratio (~17 %). Studied using ADSA-CB at 37 °C

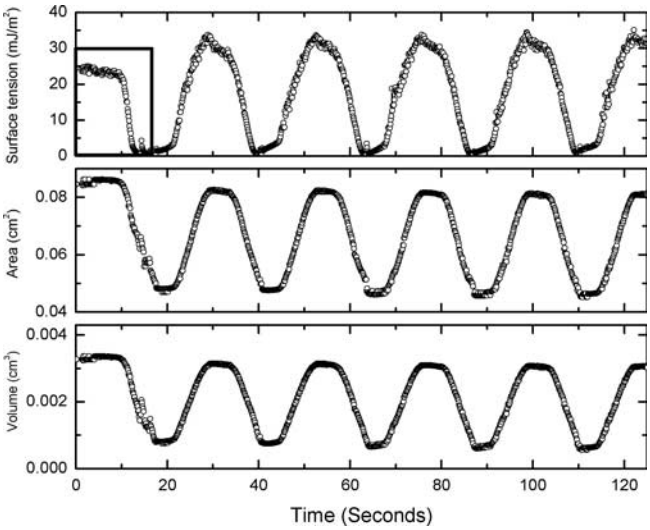

Figure 10 VAST isotherms for a dynamic cycling experiment. The dynamic experiment was conducted at a low frequency of 3 cycles/min for 5.0 mg/mL BLES. Studied using ADSA-CSD at 23 °C

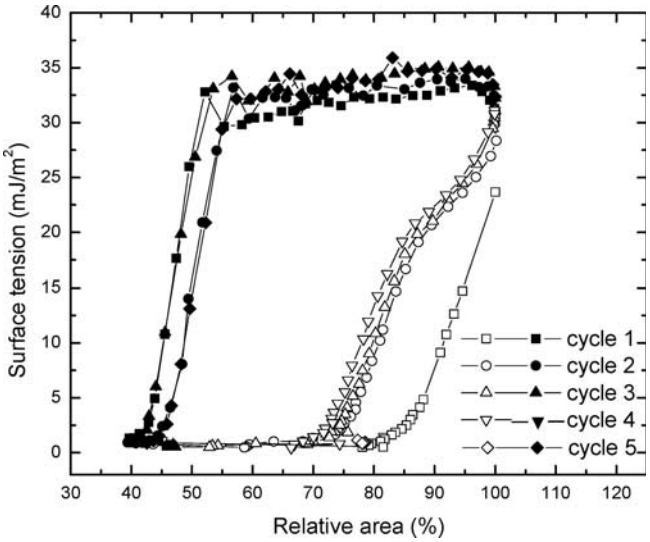

Figure 9 SA isotherms of irreversible cycling, showing pronounced hysteresis loops of compression (open symbols) and expansion (solid symbols) portions in each cycle. The experiment was conducted at a high compression ratio (~62 %). Studied using ADSA-CB at 37 °C

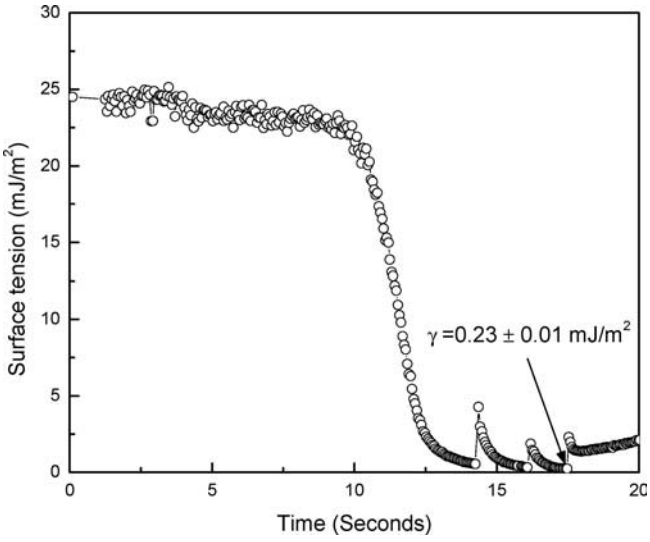

Figure 11 Enlargement of the rectangular region shown in Fig. 10. The first compression shows patterns of film collapse (indicated by the sudden increases of surface tensions). Studied using ADSA-CSD at 23 °C

lapse region. The expansion plateau occurs at the surface tension of 30–35 mJ m^{-2}, in which the effect of film dilation is balanced by replenishment of the lung surfactant molecules from the subphase or from multilayer structures associated with the interface.

It is clear that different CRs lead to different patterns of SA isotherms. At a low CR corresponding to normal physiological conditions (i. e. < 30 % [113]), no hystersis occurs. In contrast, considerable hysteresis occurs at a high CR. Hysteresis is not favorable since it causes a loss of mechanical work [213]. This may be a concern for mechanically ventilated lungs.

6.3 Very low surface tensions at high surfactant concentrations

Preliminary experiments were performed using ADSA-CSD at 23 °C [191]. A drop of BLES at 5.0 mg mL^{-1} was cycled at a relatively slow frequency (3 cycles min^{-1}). Volume-area-surface tension vs. time (VAST) isotherms for the first five cycles are shown in Fig. 10. It is noted that near-zero surface tensions are readily achieved. Fig. 11 is the enlargement of the rectangular region in Fig. 10, showing the surface tensions during the first compression. Fig. 11 clearly shows patterns of film collapse as indicated by the three jumps, i. e. sudden increase and steady decrease in surface tensions. The most important point to be noted in Fig. 11 is that a surface tension as low as 0.23 ± 0.01 mJ m^{-2} is recorded during the first compression. The results clearly demonstrate that there is no evidence of film leakage and near-zero surface tensions can be readily observed by using ADSA-CSD.

To simulate physiological conditions more closely, BLES at 5.0 mg mL^{-1} was also studied at 37 °C [191]. The lung surfactant films were cycling at a frequency of 20 cycles/min and a CR of approximately 18 %. Typical results are shown

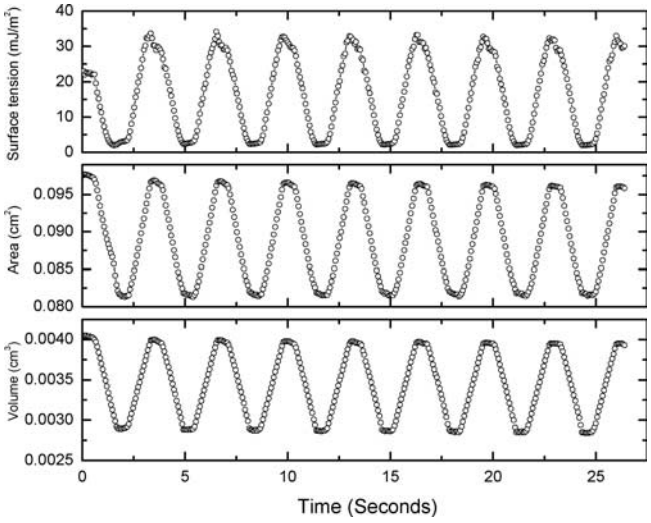

Figure 12 VAST isotherms for a dynamic cycling experiment. The dynamic experiment was conducted at a high frequency of 20 cycles/min for 5.0 mg/mL BLES. Studied using ADSA-CSD at 37 °C

in Fig. 12. It is noted that a minimum surface tension of approximately 1 mJ m^{-2} can be readily obtained in the first cycle.

6.4 Enhancement of film formation by nonionic polymers

As mentioned before, surfactant replacement has been used as a standard therapeutic intervention to RDS. However it is an expensive therapy at about US$ 500 per dose [12]. Multiple doses and continuous supply are usually required in clinical practice [12]. In contrast to the success in RDS, the surfactant replacement therapy produces less or no apparent benefit in ARDS. Inhibition of surfactant contributes partially to this poor performance. Inhibition of surfactant is defined as a process that interferes with phospholipid adsorption to form a lung surfactant film and/or prevents the film from being enriched in DPPC upon compression [214]. Two distinctive mechanisms of surfactant inhibition have been recognized [10]. They are: 1) exclusion of phospholipids from entering the interface by competitive adsorption (e. g. by plasma proteins); and 2) penetration of the surfactant film by extraneous lipids (e. g. meconium-derived free fatty acids). The former inhibition can be largely overcome by raising surfactant concentrations; however, the latter cannot be reversed by simply increasing surfactant concentrations [10].

With the goal to lower the cost of surfactant replacement therapy and to resist surfactant inhibition due to inactivating substances, recent studies [215] suggested the use of nonionic polymers, such as dextran, polyethylene glycol (PEG), and polyvinypyrrolidone (PVP), as additives to therapeutic surfactant preparations. These polymers are hoped to perform some of the functions of SP-A. The latter is absent from the currently available therapeutic surfactants. By inducing and maintaining large phospholipid aggregation, SP-A is able to enhance adsorption of a dilute surfactant preparation and, more importantly, resist surfactant inhibitors, most likely due to a competitive adsorption mechanism. Previous studies found that the carbohydrate recognition domain of SP-A is responsible for its ability to interact with phospholipid liposomes [33, 216, 217]. Therefore, one expects that the efficacy of the present formulations for surfactant replacement therapy can be improved by adding simple sugars, sugar based polymers, or other nonionic polymers.

Both *in vitro* [185, 187, 188, 215, 218] and *in vivo* [219–221] experiments showed that the addition of the nonionic polymers can significantly improve the efficacy of a therapeutic surfactant at least in two ways: 1) by enhancing the surface activityof a dilute surfactant preparation; and 2) by reversing the surfactant inhibition due to a number of substances, such as plasma proteins and meconium. The role of nonionic polymers in resisting the inhibitory substances and its application in the treatment of ARDS were recently reviewed [214, 222].

Among the tested nonionic polymers, PEG was found to be the most efficient one [215]. PEG is a linear or branched, neutral polyether, available in a variety of molecular weights [223]. At high molecular weight (> 20 000), PEG is also frequently referred to as poly(ethylene oxide) (PEO). PEG is soluble in water and most organic solvents. It is nontoxic and has been approved by the United States Food and Drug Administration (FDA) for internal consumption. PEG is readily attached to other molecules (e. g. proteins) and surfaces (e. g. cell membranes); however, PEG has little effect on the chemical properties of these molecules but controls their aggregation and solubility [223]. These properties of PEG caused considerable interest in a variety of biological, biomedical and biomaterial applications, such as cell fusion, drug delivery, and surface modification in order to prevent protein and cell adhesion. Applications of PEG were summarized by Zalipsky and Harris [224].

ADSA methods were used to study the effect of PEG on the surface activity of lung surfactant. Both adsorption [185] and dynamic cycling [188] were studied using different experimental strategies. These studies confirmed that the addition of PEG can enhance the surface activity of a therapeutic lung surfactant. For example, using ADSA-CB, the dynamic stability of PEG-enhanced BLES films were tested [188]. It was found that PEG can significantly improve the stability of BLES films, thus producing less hysteresis and lower minimum surface tensions during compression. Moreover, PEG is capable of restoring a surfactant film after its collapse, presumably by enhancing the readsorption and respreading of surface active materials or by strengthening the "surfactant-associated reservoir", just as SP-A does [68].

Using ADSA-PD, the effect of PEG on the adsorption of BLES at a dilute concentration was studied. Fig. 13 shows the adsorption kinetics of 0.5 mg mL^{-1} natural surfactant, 0.5 mg mL^{-1} BLES, and to which PEG (MW 10 000) at a variety of concentrations was added. It is noted that the adsorption of natural surfactant, i. e. endogenous surfactant with complete surfactant components including SP-A, is so fast that the equilibrium surface tensions are reached within less than 10 s. In contrast, the adsorption of BLES (i. e. an exogenous surfactant without SP-A) at the same concentration as the natural surfactant is very slow. It takes approximately 200 s to reach equilibrium. The adsorption of BLES can be significantly enhanced by adding PEG and this enhancement is PEG concentration dependent. It is also clear from Fig. 13 that the improved surface activity is not due to adsorption of PEG since the surface tension of dissolved PEG alone remains constant at about 58 mJ m^{-2}. Particularly, at a PEG concentration of 28 mg mL^{-1}, the mixture of BLES and PEG shows greatly improved adsorption kinetics, close to that of the natural lung surfactant.

The experimental results also imply that 28 mg mL^{-1} is an optimal concentration for PEG (MW 10 000) in terms of adsorption enhancement because further increasing the PEG concentration yields no apparent improvement in the adsorption rate of BLES. This is more clearly demonstrated in Fig. 14, which shows the surface tension measured im-

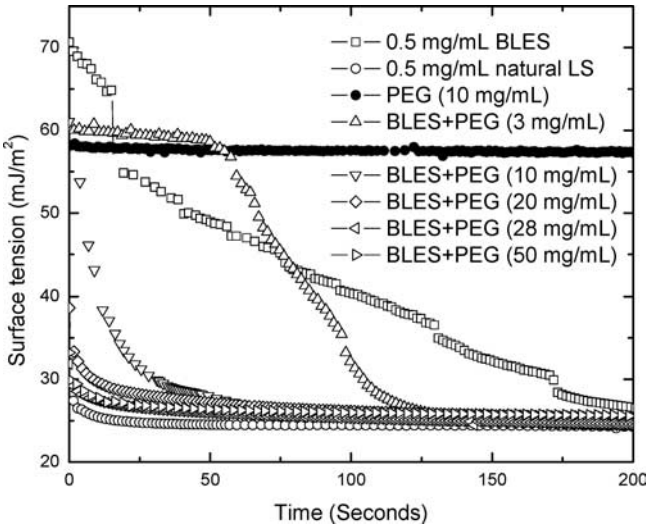

Figure 13 Effect of PEG (MW 10, 000) concentrations on the adsorption kinetics of 0.5 mg/mL BLES. Studied using ADSA-PD at 37 °C

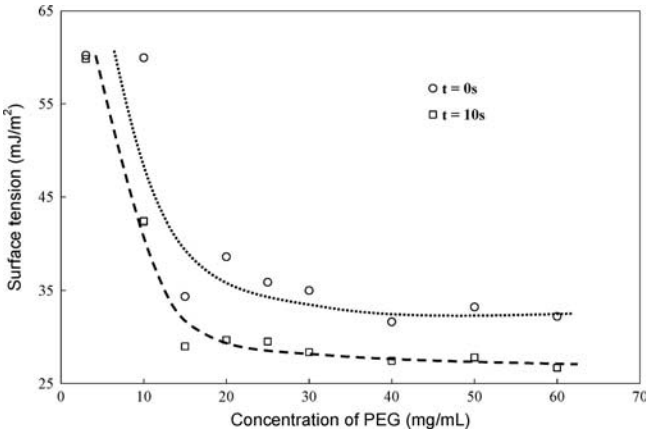

Figure 14 Effect of PEG (MW 10,000) concentrations on the surface tensions at time zero and after 10 s of adsorption. Studied using ADSA-PD at 37 °C

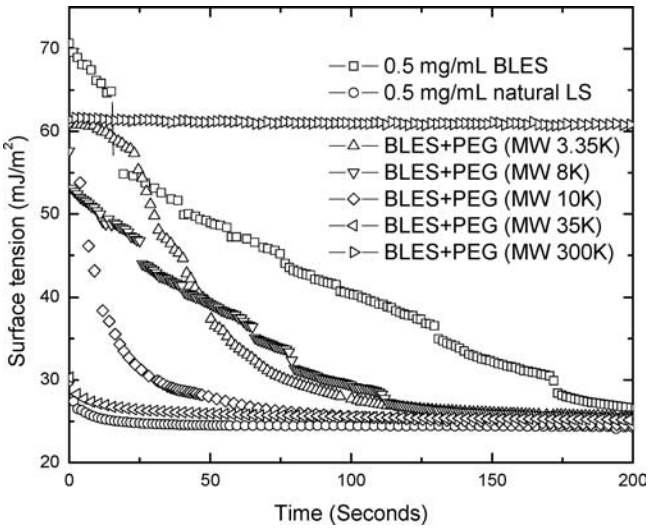

Figure 15 Effect of PEG (10 mg/mL) molecular weights on the adsorption kinetics of 0.5 mg/mL BLES. Studied using ADSA-PD at 37 °C

mediately after drop formation (t = 0 s) and after 10 s of adsorption (t = 10 s) as a function of PEG concentrations. Also implied by Fig. 14 is that a minimum PEG (MW 10 000) concentration of about 10 mg mL^{-1} is required to produce detectable enhancement in BLES adsorption.

The ability of PEG to enhance the adsorption of BLES at a low concentration was found to be also dependent on its molecular weight. Fig. 15 shows the adsorption curves of 0.5 mg mL^{-1} BLES to which PEG at 10 mg mL^{-1} but with different molecular weights was added. It appears to have an effective range of molecular weight, i. e. 3 350 – 35 000, in which PEG at the chosen concentration of 10 mg mL^{-1} is able to enhance BLES adsorption. PEG with a molecular weight out of this range, e. g. 300 000, shows no enhancement in BLES adsorption.

The improvement of PEG on BLES adsorption may be due to its ability to induce large phospholipid aggregates [185]. It is known that large aggregates are more surface active than their small counterparts [150, 225]. Generally, it has been known for a long time that polymers are able to promote surfactant aggregates by destabilizing surfactant dispersions [226, 227]. Specifically, PEG at a certain molecular weight and concentration shows the ability to induce large aggregates in a pure PC vesicle system, most likely due to a PEG-induced depletion attraction force [228, 229]. Direct surface force measurement in the pure PC vesicle system showed that only PEG within a moderate range of molecular weight (i. e. 8 000~10 000) is able to yield a depletion attraction force significant enough to induce aggregation [228]. Low molecular weight PEG (<1 000) is ineffective; and, high molecular weight PEG (>20 000) shows only repulsive force [228]. The molecular weight dependence in the adsorption studies of lung surfactant is somewhat different.

Apart from the molecular weight, a critical polymer concentration has to be reached to induce PC aggregation [229]. This critical concentration was found to be close to the overlapping concentration of the polymer [229]. At the overlapping concentration, the polymer molecules start to interact and entangle with each other [230]. This critical concentration decreases with increasing molecular weight. For PEG with MW 10 000, 28 mg mL^{-1} was found to be this critical concentration [228]. At this molecular weight and concentration the best performance of PEG in terms of enhancing BLES adsorption was found, although a detectable favorable effect by adding PEG can be observed at a lower concentration (i. e. approximately 10 mg mL^{-1} as shown in Fig. 14). All of the evidence strongly suggests that the PEG-induced depletion attraction force may be responsible for the enhanced adsorption rate observed in the current polymer-lung surfactant system.

It is concluded that the addition of PEG can enhance the adsorption of exogenous lung surfactant. The enhancement is simultaneously dependent on the concentration and the molecular weight of PEG. It is also suggested that an optimal concentration may be close to the overlapping concentration for certain polymers with a certain molecular weight. However, it is also important to note that the optimal polymer concentration determined from this study is solely based on the evaluation of *in vitro* surface tension performance. Optimal polymer concentrations will ultimately also require physiological considerations, such as the efficacy of the tracheal instillation [214] and the effect of the additional polymers on pulmonary gas exchange [231].

7 Summary and perspectives

The accuracy, versatility, and simplicity of ADSA methods facilitate various studies of lung surfactant. In conjunction

with different drop/bubble configurations, i. e. PD, CB, and CSD, ADSA methods are able to assess the *in vitro* surface tension characteristics of lung surfactant related systems. These characteristics are rapid film formation, very low surface tension with extremely low film compressibility, high dynamic film stability and enhancement of surface activity due to the addition of nonionic polymers.

Along the lines discussed above, ADSA methods can be extended to further studies of lung surfactant. For instance, by examining dynamic surface tensions during adsorption, ADSA-PD can be used to study the molecular interaction between phospholipids and lung surfactant associated proteins. ADSA-CB can be used to study the effect of lung surfactant film and polymer-enhanced film on the pulmonary gas exchange. Preliminary results suggest that the gas transfer properties of polymer-enhanced lung surfactant films are dependent on the polymer concentration [232]. ADSA-CSD is promising in the study of dynamic surface activity of lung surfactant films adsorbed at physiologically relevant concentrations. Patterns of surface tension significantly different from those at low surfactant concentrations were observed [233]. Even more interesting is the inference from the comparison among these different experimental methodologies. For instance, a comparison of adsorption kinetics among PD, CB and CSD implies that gravity may play a role in the *in vitro* film formation of lung surfactant [234].

Acknowledgements

This work was supported by a grant from Canadian Institutes of Health Research (MOP-38037) and an Open Fellowship from University of Toronto to YYZ. We also thank Dr. David Bjarneson of BLES Biochemicals Inc. for his generous donation of the BLES samples.

References

1. *West, J. B.*: Respiratory Physiology-the Essentials, 6th edn. (2000) Lippincott Williams & Wilkins, Baltimore.
2. *Lumb, A. B.*: Nunn's Applied Respiratory Physiology, 5th edn. (2000) Butterworth-Heinemann, Oxford.
3. *Weibel, E. R.* and *Gil, J.*: Respir. Physiol. *4* (1968) 42.
4. *Clements, J. A.*: Physiologist *5* (1962) 11.
5. *Clements, J. A.*: Am. Rev. Respir. Dis. *115* (1977) 67.
6. *Hildebran, J. N., Goerke, J.* and *Clements, J. A.*: J. Appl. Physiol. *47* (1979) 604.
7. *Fung, Y. C.*: Biomechanics, Motion, Flow, Stress, and Growth (1990) Sprinder-Verlag, New York.
8. *Notter, R. H.*: Lung Surfactant, Basic Science and Clinical Application (2000) Marcel Dekker, New York.
9. *Lewis, J. F.* and *Veldhuizen, R.*: Annu. Rev. Physiol. *65* (2003) 613.
10. *Holm, B. A., Wang, Z. D.* and *Notter, R. H.*: Pediatr. Res. *46* (1999) 85.
11. *McIntyre, Jr. R. C., Pulido, E. J., Bensard, D. D., Shames, B. D.* and *Abraham, E.*: Crit. Care Med. *28* (2000) 3314.
12. *Robertson, B.* and *Haliday, H. L.*: Biochim. Biophys. Acta *1408* (1998) 346.
13. *Rotenberg, Y., Boruvka, L.* and *Neumann, A. W.*: J. Colloid Interface Sci. *93* (1983) 169.
14. *Cheng, P., Li, D., Boruvka, L., Rotenberg, Y.* and *Neumann, A. W.*: Colloids Surfaces *43* (1990) 151.
15. *del Río, O. I.* and *Neumann, A. W.*: J. Colloid Interface Sci. *196* (1997) 136.
16. *Hoorfar M.* and *Neumann A. W.*: Axisymmetric Drop Shape Analysis (ADSA) for the determination of surface tension and contact angle. J. Adhesion *80* (2004) 727–743.
17. *Zuo, Y. Y., Ding, M., Bateni, A., Hoorfar, M.* and *Neumann, A. W.*: Colloids Surfaces A: Physicochem. Eng. Aspects *250* (2004) 233.
18. *Zuo, Y. Y., Ding, M., Li, D.* and *Neumann, A. W.*: Biochim. Biophys. Acta *1675* (2004) 12.
19. *Kwok, D. Y., Cabrerizo-Vílchez, M. A., Gomez, Y., Susnar, S. S., del Río, O., Vollhardt, D., Miller, R.* and *Neumann, A. W.*: in Pillai, V. and Shah D. O. (Eds.), Dynamic Properties of Interfaces and Association Structures (1996) Champaign, pp. 278.
20. *Kwok, D. Y., Chiefalo, P., Khorshiddoust, B., Lahooti, S., Cabrerizo-Vílchez, M. A., del Río, O.* and *Neumann, A. W.*: in Sharma, R. (Ed.), Surfactant Adsorption and Surface Solubilization (1995) Washington, pp. 374.
21. *Kwok, D. Y., Vollhardt, D., Miller, R., Li, D.* and *Neumann, A. W.*: Colloids Surfaces A: Physicochem. Eng. Aspects *88* (1994) 51.
22. *Daniels, C. B.* and *Orgeig, S.*: Comp Biochem Physiol A *129* (2001) 9.
23. *Goerke, J.*: Biochim. Biophys. Acta *344* (1974) 241.
24. *Whitsett, J. A.*: in: Polin, R. A. and Fox, W. W. (Eds), Fetal and Neonatal Physiology, 2nd edn (1992) WB Saunders Company, Philadelphia, pp. 941.
25. *Possmayer, F.*: in: Polin, R. A. and Fox, W. W. (Eds), Fetal and Neonatal Physiology, 2nd edn (1992) WB Saunders Company, Philadelphia, pp. 949.
26. *Possmayer, F.*: Am. Rev. Respir. Dis. *138* (1988) 990.
27. *Goerke, J.* and *Clements, J. A.*: in Macklem, P. T. and Mead, J. (Eds.), Handbook of Physiology: The Respiratory System (1986) American Physiology Society, Bethesda, pp. 247.
28. *Goerke, J.* and *Gonzales, J.*: J. Appl. Physiol. *51* (1981) 1108.
29. *Veldhuizen, R., Nag, K., Sandra, O.* and *Possmayer, F.*: Biochim. Biophys. Acta *1408* (1998) 90.
30. *Veldhuizen, E. J. A.* and *Haagsman, H. P.*: Biochim. Biophys. Acta *1467* (2000) 255
31. *Pérez-Gil, J.* and *Keough, K. M. W.*: Biochim Biophys Acta *1408* (1998) 203.
32. *Goerke, J.*: Biochim. Biophys. Acta *1408* (1998) 79.
33. *McCormack, F. X.*: Biochim Biophys Acta *1408* (1998) 109.
34. *Yu, S. H.* and *Possmayer, F.*: Biochim. Biophys. Acta *1046* (1990) 233.
35. *Pison, U., Shiffer, K., Hawgood, S.* and *Goerke, J.*: Prog. Respir. Res. *25* (1990) 271.
36. *Yu, S. H.* and *Possmayer, F.*: Biochim. Biophys. Acta *1211* (1994) 350.
37. *Venkitaraman, A. R., Hall, S. B., Whitsett, J. A.* and *Notter, R. H.*: Chem. Phy. Lipids *56* (1990) 185.
38. *Chung, J., Yu, S. H., Whitsett, J. A., Harding, P. G. R.* and *Possmayes, F.*: Biochim. Biophys. Acta *1002* (1989) 348.
39. *Cockshutt, A. M., Weitz, J.* and *Possmayer, F.*: Biochem. J. *29* (1990) 8424.
40. *Schürch, S., Possmayer, F., Cheng, S.* and *Cockshutt, A. M.*: Am. J. Physiol. *263* (1992) L210.
41. *Sun, B., Curstedt, T., Lindgren, G., Franzén, B., Alaiya, AA., Calkovská, A.* and *Robertson, B.*: Eur Respir J. *10* (1997) 1967.
42. *Suzuki, Y., Fujita, Y.* and *Kogishi, K.*: Am. Rev. Respir. Dis. *140* (1989) 75.
43. *Veldhuizen, R. A. W., Yao, L. J., Hearn, S. A., Possmayer, F.* and *Lewis, J. F.*: Biochem. J. *313* (1996) 835.
44. *Wright, J. R., Wager, R. E., Hawgood, S., Dobbs, L.* and *Clements, J. A.*: J. Biol. Chem. *262* (1987) 2888.
45. *Mason, R. J., Greene, K.* and *Voelker, D. R.*: Am. J. Physiol. *275* (1998) L1.
46. *Hawgood, S., Derrick, M.* and *Poulain, F.*: Biochim. Biophys. Acta *1408* (1998) 150.
47. *Nag, K., Munro, J. G., Inchley, K., Schürch, S., Petersen, N. O.* and *Possmayer F.*: Am. J. Physiol. *277* (1999) L1179.
48. *Johansson, J.*: Biochim. Biophys. Acta *1408* (1998) 161.
49. *Putz, G., Walch, M., Van Eijk, M.* and *Haagsman, H. P.*: Biochim. Biophys. Acta *1453* (1999) 126.
50. *Veldhuizen, E. J., Diemel, R. V., Putz, G., van Golde, L. M., Batenburg, J. J.* and *Haagsman, H. P.*: Chem. Phys. Lipids *110* (2001) 47.
51. *Crouch, E. C.*: Biochim. Biophys. Acta *1408* (1998) 278.
52. *Goerke, J.*: in: Robertson, B., van Golde, L. M. G. and Batenburg J. J. (Eds), Pulmonary Surfactant: from Molecular Biology to Clinical Practice (1992) Elsevier, New York, pp. 165.
53. *Keough, K. M. W.*: in: Robertson, B., van Golde, L. M. G. and Batenburg, J. J. (Eds), Pulmonary Surfactant: from Molecular Biology to Clinical Practice (1992) Elsevier, New York, pp. 109.
54. *Pison, U., Herold, R.* and *Schürch, S.*: Colloids and surface A: Physicochem. Eng. Aspects *114* (1996) 163.
55. *Hawgood, S.*: in Crystal, R. G. and West, J. B. et al. (Eds), The Lung: Scientific Foundations, 2nd ed (1997) Lippincott-Raven, Philadelphia, pp. 557.
56. *Creuwels, L. A. J. M., van Golde, L. M. G.* and *Haagsman, H. P.*: Lung *175* (1997) 1.
57. *Keough, K. M. W.*: in Rooney, S. A. (Ed) Lung Surfactant: Cellular and Molecular Processing (1998) R. G. Landes, Austin, pp. 1.
58. *Haagsman, H. P.* and *Diemel, R. V.*: Comp. Biochem. Physiol. A *129* (2001) 91.
59. *Possmayer, F., Nag, K., Rodriguez, K., Qanbar, R.* and *Schürch, S.*: Comp. Biochem. Physiol. A *129* (2001) 209.
60. *Gil, J.* and *Weibel, E. R.*: Respir. Physiol. *8* (1969) 13.
61. *Untersee, P., Gil, J.* and *Weibel, E. R.*: Respir Physiol. *13* (1971) 171.
62. *Bastacky, J., Lee, C. Y., Goerke, J., Koushafar, H., Yager, D., Kenaga, L., Speed, T. P., Chen, Y.* and *Clements, J. A.*: J Appl Physiol. *79* (1995) 1615.
63. *Notter, R. H.* and *Jacob, N. F.*: J. Appl. Physiol. *57* (1984) 1613.
64. *Clements, J. A., Brown, E. S.* and *Johnson, R. P.*: J. Appl. Physiol. *12* (1958) 262.
65. *Pattle, R. E.*: Physiol Rev. *45* (1965) 48.
66. *Schürch, S., Bachofen, H.* and *Possmayer, F.*: in: Hlastala, M. P. and Robertson H. T. (Eds), Complexities in Structure and Function of the Lung (In series: C. Lenfant (Ed.), Lung Biology in Health and Disease, vol. 121) (1998) Marcel Dekker, New York, pp. 35.
67. *Schürch, S., Green, F. H. Y.* and *Bachofen H.*: Biochim. Biophys. Acta *1408* (1998) 180.
68. *Schürch, S., Qanbar, R., Bachofen, H.* and *Possmayer F.*: Biol. Neonate *67* (1995) 61.
69. *Schürch, S.* and *Bachofen, H.*: in: Robertson, B. and Taeusch H. W. (Eds), Surfactant Therapy for Lung Disease (In series: C. Lenfant (Ed.), Lung Biology in Health and Disease, vol. 84) (1995) Marcel Dekker, New York, pp. 3.
70. *Grunder, R., Gehr, P., Bachofen, H., Schürch, S.* and *Siegenthaler H.*: Eur. Respir. J. *14* (1999) 1290.
71. *Schürch, S., Schürch, D., Curstedt, T.* and *Robertson, B.*: J. Appl. Physiol. *77* (1994) 974.
72. *Piknova, B., Schram, V.* and *Hall, S. B.*: Curr. Opin. Structural Biology *12* (2002) 487.
73. *Schürch, S., Bachofen, H.* and *Possmayer F.*: Comp. Biochem. Physiol. A *129* (2001) 195.

74. *Baritussio, A. G., Magoon, M. W., Goerke, J.* and *Clements, J. A.*: Biochim. Biophys. Acta *666* (1981) 382.
75. *Fisher, A. B.*: in: Rooney, S. A. (Ed) Lung Surfactant: Cellular and Molecular Processing (1998) R.G. Landes, Austin, pp. 165.
76. *Wright, J. R.* and *Clements, J. A.*: Am. Rev. Respir. Dis. *136* (1987) 426.
77. *Veldhuizen, R.* and *Possmayer, F.*: Subcell Biochem. *37* (2004) 359.
78. *von Neergaard, K.*: Neue auffassungen über einen grundbegriff der atemmechanik. Z. Ges. Exp. Med. *66* (1929) 1.
79. *Pattle, R. E.*: Nature *175* (1955) 1125.
80. *Pattle, R. E.* and *Thomas, L. C.*: Nature *189* (1961) 844.
81. *Mead, J., Whittenberger, J. L.* and *Radford, Jr., E. P.*: J. Appl. Physiol. *10* (1957) 191.
82. *Clements, J. A.*: Proc. Soc. Exp. Biol. Med. *95* (1957) 170.
83. *Schürch, S., Goerke, J.* and *Clements, J. A.*: Proc. Natl. Acad. Sci. USA *73* (1976) 4689.
84. *Clements, J. A.*: In: History of Respiratory Physiology, West J. (Ed) (1996) Oxford Univ. Press, New York, pp. 208.
85. *Clements, J. A.*: Annu. Rev. Physiol. *59* (1997) 1.
86. *Avery, M. E.* and *Mead, J.*: Am. J. Dis. Child. 97 (1959) 517.
87. *Brumley, G. W., Chernick, V., Hodson, W. A., Normand, C., Fenner, A.* and *Avery, M. E.*: J. Clin. Invest. *46* (1967) 863.
88. *Brown, E. S.*: Am. J. Physiol. *207* (1964) 402.
89. *Chu, J., Clements, J. A., Cotton, E. K., Klaus, M. H., Sweet, A. Y., Tooley, W. H., Bradley, B. L.* and *Brandorff, L. C.*: Pediatrics *40* (1967) 709.
90. *King, R. J.*: Fed. Proc. *33* (1974) 2238.
91. *Fujiwara, T., Maeta, H., Chida, S., Morita, T., Watabe, Y.* and *Abe, T.*: Lancet *1* (8159) (1980) 55.
92. *Schoendorf, K. C.* and *Kiely, J. L.*: Arch. Pediatr. Adolesc. Med. *151* (1997) 129.
93. *Guyer, B., Freedman, M. A., Strobino, D. M.* and *Sondik, E. J.*: Pediatrics *106* (2000) 1307.
94. *Ashbaugh, D. G., Bigelow, D. B., Petty, T. L.* and *Levine, B. E.*: Lancet *2* (7511) (1967) 319.
95. *Petty, T. L.* and *Ashbaugh, D. G.*: Chest *60* (1971) 233.
96. *Gregory, T. J., Steinberg, K. P., Spragg, R., Gadek, J. E., Hyers, T. M., Longmore, W. J., Moxley, M. A., Cai, G. Z., Hite, R. D., Smith, R. M., Hudson, L. D., Crim, C., Newton, P., Mitchell, B. R.* and *Gold, A. J.*: Am. J. Respir. Crit. Care Med. *155* (1997) 1309.
97. *Haitsma, J. J., Papadakos, P. J.* and *Lachmann, B.*: Curr. Opin. Crit. Care *10* (2004) 18.
98. *Baudouin, S. V.*: N. Engl. J. Med *351* (2004) 853.
99. *Lewis, J. F.* and *Jobe, A. H.*: Am. J. Respir. Crit. Care Med. *147* (1993) 218.
100. *Hamm, H., Kroegel, C.* and *Hohlfeld, J.*: Respir. Med *90* (1996) 251.
101. *Clements, J. A.* and *Avery, M. E.*: Am. J. Respir. Crit. Care Med *157* (1998) S59.
102. *Frerking, I., Günther, A., Seeger, W.* and *Pison, U.*: Intensive Care Med *27* (2001) 1699.
103. *Lewis, J. F.* and *Brackenbury, A.*: Crit. Care Med. *31* (2003) S324.
104. *Robertson, B.* and *Lachmann, B.*: Experimental Lung Research *14* (1988) 279.
105. *Robertson, B.*: in Robertson, B., van Golde, L. M. G. and Batenburg, J. J. (Eds), Pulmonary Surfactant: from Molecular Biology to Clinical Practice (1992) Elsevier, New York, pp. 459.
106. *Brown, D. L.* and *Pattishall, E. N.*: Clinics in Perinatology *20* (1993) 761.
107. *Robertson, B.*: in: Robertson, B. and Taeusch, H. W. (Eds), Surfactant Therapy for Lung Disease (1995) Marcel Dekker, New York, pp. 239.
108. *Schürch, S., Goerke, J.* and *Clements, J. A.*: Proc. Natl. Acad. Sci. USA *75* (1978) 3417.
109. *Schürch, S.*: Respir. Physiol. *48* (1982) 339.
110. *Schürch, S., Bachofen, H.* and *Weibel, E. R.*: Respir. Physiol. *62* (1985) 31.
111. *Fisher, M. J., Wilson, M. F.* and *Weber, K.C.*: Respir. Physiol. *10* (1970) 159.
112. *Bachofen, H., Hildebrant, J.* and *Bachofen, M.*: J. Appl. Physiol. *29* (1970) 422.
113. *Bachofen, H., Schürch, S., Urbinelli, M.* and *Weibel, E. R.*: J. Appl. Physiol. *62* (1987) 1878.
114. *Wilson, T. A.*: J. Appl. Physiol. *50* (1981) 921.
115. *Wilson, T. A.*: J. Appl. Physiol. *53* (1982) 1512.
116. *Prokop, R. M., Chen, P., Garg, A.* and *Neumann, A.W.*: Colloids Surfaces B: Biointerfaces *13* (1999) 59.
117. *Hills, B. A.*: The Biology of Surfactant (1988) Cambridge University Press, Cambridge.
118. *Schürch, S.*: Clinics in Perinatology *20* (1993) 669.
119. *Robertson, B.* and *Schürch, S.*: In: Uhlig, S. and Taylor, A. E. (Eds), Methods in Pulmonary Research (1998) Birkhäuser, Basel, pp. 349.
120. *Langmuir, I.*: J. Am. Chem. Soc. *39* (1917) 1848.
121. *Brown, E. S., Johnson, R. P.* and *Clements, J. A.*: J. Appl. Physiol. *14* (1959) 717.
122. *Clements, J. A., Hustead, R. F., Johnson, R. P.* and *Gribetz, I.*: J. Appl. Physiol. *16* (1961) 444.
123. *Zasadzinski, J. A., Ding, J., Warriner, H. E., Bringezu, F.* and *Waring, A. J.*: Curr. Opin. Colloid Interf. Sci. *6* (2001) 506.
124. *Discher, B. M., Maloney, K. M., Schief, W. R., Grainger, D. W., Vogel, V.* and *Hall, S. B.*: Biophys. J. *71* (1996) 2583.
125. *Lipp, M. M., Lee, K. Y. C., Zasadzinski, J. A.* and *Waring, A. J.*: Rev. Sci. Instrum. *68* (1997) 2574.
126. *Discher, B. M., Schief, W. R., Vogel, V.* and *Hall, S. B.*: Biophys. J. *77* (1999) 2051.
127. *Piknova, B., Schief, W. R., Vogel, V., Discher, B. M.* and *Hall, S. B.*: Biophys. J. *81* (2001) 2172.
128. *Amrein, M., von Nahmen, A.* and *Sieber, M.*: Europ. Biophys. J. *26* (1997) 349.
129. *von Nahmen, A., Post, A., Galla, H. J.* and *Sieber, M.*: Europ. Biophys. J. *26* (1997) 359.
130. *Nag, K., Perez-Gil, J., Ruano, M. L. F., Worthman, L. A. D., Stewart, J., Casals, C.* and *Keough, K. M. W.*: Biophys. J. *74* (1998) 2983.
131. *von Nahman, A., Schenk, M., Sieber, M.* and *Amrein, M.*: Biophys. J. *72* (1997) 463.
132. *Grunder, R., Gehr, P., Bachofen, H., Schürch, S.* and *Siegenthaler, H.*: Eur. Respir. J. *14* (1999) 1290.
133. *Nag, K., Munro, J. G., Hearn, S. A., Rasmusson, J., Petersen, N. O.* and *Possmayer, F.*: J. Stru. Biol. *126* (1999) 1.
134. *Panda, A. K., Nag, K., Harbottle, R. R., Rodriguez-Capote, K., Veldhuizen, R. A. W., Petersen, N. O.* and *Possmayer, F.*: Am. J. Respir. Cell Biol. *30* (2004) 641.
135. *Adamson, A. W.*: Physical Chemistry of Surfaces, 5th edn (1990) Wiley, New York.
136. *Hills, B. A.*: J. Physiol. *359* (1985) 65.
137. *Prokop, R. M.* and *Neumann, A. W.*: Curr. Opin. Colloid Interf. Sci. *1* (1996) 677.
138. *Tabak, S. A.* and *Notter, R. H.*: Rev. Sci. Instrum. *48* (1977) 1196.
139. *Goerke, J.* and *Gonzales, J.*: J. Appl. Physiol. *51* (1981) 1108.
140. *Enhorning, G.*: J. Appl. Physiol. *43* (1977) 198.
141. *Putz, G., Goerke, J., Taeusch, H. W.* and *Clements, J. A.*: J. Appl. Physiol. *76* (1994) 1425.
142. *Hall, S. B., Bermel, M. S., Ko, Y. T., Palmer, H. J., Enhorning, G. A.* and *Notter, R. H.*: J. Appl. Physiol. *75* (1993) 468.
143. *Chang, C. H.* and *Franses, E. I.*: J. Colloid Inf. Sci. *164* (1994) 107.
144. *Schürch, S., Bachofen, H., Goerke J.* and *Possmayer F.*: J. Appl. Physiol. *67* (1989) 2389.
145. *Schürch, S., Bachofen, H., Goerke, J.* and *Green, F.*: Biochim. Biophys. Acta *1103* (1992) 127.
146. *Putz, G.* and *Walch, M.*: Biophys. J. *75* (1998) 2229.
147. *Putz, G., Goerke, J., Schürch, S.* and *Clements, J. A.*: J. Appl. Physiol. *76* (1994) 1417.
148. *Schoel, W. M., Schürch, S.* and *Goerke, J.*: Biochim. Biophys. Acta *1200* (1994) 281.
149. *Malcolm, J. D.* and *Elliott, C. D.*: Can. J. Chem. Eng. *58* (1980) 151.
150. *Putz, G., Goerke, J.* and *Clements, J.A.*: J. Appl. Physiol. *77* (1994) 597.
151. *Exerowa, D., Lalchev, Z., Marinov, B.* and *Orgnyanov, K.*: Langmuir *2* (1986) 664.
152. *Exerowa, D., Kashchiev, D.* and *Platikanov, D.*: Adv. Colloid Interface Sci. *40* (1992) 201.
153. *Berggren, P., Eklind, J., Linderholm, B.* and *Robertson, B.*: Biol. Neonate. *61* (1992) 15.
154. *Skelton, R.* and *Jeffery, H.*: Pediatr. Pulmonol. *17* (1994) 383.
155. *Cho, K., Chida, S., Sasaki, M.* and *Fujiwara, T.*: Acta Paediatr. Jpn. *38* (1996) 322.
156. *Cordova, M., Mautone, A. J.* and *Scarpelli, E. M.*: Pediatr. Pulmonol. *21* (1996) 373.
157. *Verder, H., Ebbesen, F., Linderholm, B., Robertson, B., Eschen, C., Arroe, M., Lange, A., Grytter, C., Bohlin, K.* and *Bertelsen., A.*: Acta Paediatr. *92* (2003) 728.
158. *Chung, J. B., Shanks, P. C., Hanneman, R. E.* and *Franses, E. I.*: Colloids Surf. *43* (1990) 223.
159. *Enhorning, G.* and *Holm, B. A.*: J. Appl. Physiol. *74* (1993) 2922.
160. *Enhorning, G.*: Comp. Biochem. Physiol. A *129* (2001) 221.
161. *Lahooti, S., del Río, O. I., Cheng, P.* and *Neumann, A. W.*: in: Neumann, A. W. and Spelt, J. K. (Eds) Applied Surface Thermodynamics (1996) Marcel Dekker, New York, pp. 441.
162. *Voigt, A., Thiel, O., Williams, D., Policova, Z., Zingg, W.* and *Neumann, A. W.*: Colloids Surf. *58* (1991) 315.
163. *Miller, R., Treppo, S., Voigt, A., Zingg, W.* and *Neumann, A. W.*: Colloids Surf. *69* (1993) 203.
164. *Miller, R., Sedev, R. V., Schano, K. H., Ng, C.* and *Neumann, A. W.*: Colloids Surf. *69* (1993) 209.
165. *Chen, P., Policova, Z., Susnar, S. S., Pace-Asciak, C. R., Demin, P. M.* and *Neumann, A. W.*: Colloids Surfaces A: Physicochem Eng Aspects *114* (1996) 99.
166. *Chen, P., Policova, Z., Pace-Asciak, C. R.* and *Neumann, A. W.*: J. Pharm. Sci. *88* (1999) 1293.
167. *Chen, P., Policova, Z., Pace-Asciak, C. R.* and *Neumann, A. W.*: Colloids Surfaces B: Biointerfaces *15* (1999) 313.
168. *Jyoti, A., Prokop, R. M.* and *Neumann, A. W.*: Colloids Surfaces B: Biointerfaces *8* (1997) 115.
169. *Busscher, H. J., van der Vegt, W., Noordmans, J., Schakenraad, J. M.* and *van der Mei, H. C.*: Colloid Surf. *58* (1991) 229.
170. *Siboni, S., Della, V. C., Maniglio, D.* and *Brugnara, M.*: J. Colloid Interface Sci. *271* (2004) 454.
171. *Hong, Y., Legge, R. L., Zhang, S.* and *Chen, P.*: Biomacromolecules *4* (2003) 1433.
172. *Rosales-Leal, J. I., Osorio, R., Toledano, M., Cabrerizo-Vilchez, M. A.* and *Millstein, P. L.*: Oper. Dent. *28* (2003) 695.
173. *Wege, H. A., Aguilar, J. A., Rodriguez-Valverde, M. A., Toledano, M., Osorio, R.* and *Cabrerizo-Vilchez, M. A.*: J Colloid Interface Sci. *263* (2003) 162.
174. *Ferraz, M. P., Monteiro, F. J., Serro, A. P., Saramago, B., Gibson, I. R.* and *Santos, J. D.*: Biomaterials *22* (2001) 3105.
175. *Crane, J. M., Putz, G.* and *Hall, S. B.*: Biophys. J. *77* (1999) 3134.
176. *Wüstneck, N., Wüstneck, R., Fainerman, V. B., Miller, R.* and *Pison, U.*: Colloids Surf. B: Biointerfaces *21* (2001) 191.
177. *Wüstneck, N., Wüstneck, R.* and *Pison, U.*: Langmuir *19* (2003) 7521.
178. *Thiessen, D. B.* and *Man, K. F.*: in Webster, J. G. (Ed), The Measurement, Instrumentation, and Sensors Handbook (1999) CRC Press: IEEE Press, Boca Raton, pp. 31.1.
179. *Thiessen, D. B.* and *Man, K. F.*: in Webster, J. G. (Ed), Mechanical Variables Measurement: Solid, Fluid, and Thermal (2000) CRC Press, Boca Raton, pp. 12.1.

180. *Susnar, S. S.* and *Neumann, A. W.*: CSME Transactions *24* (2000) 215.
181. *Hoorfar, M., Kruz, M. A.* and *Neumann, A. W.*: Colloids Surfaces A: Physicochem. Eng. Aspects, in press.
182. *Li, D., Cheng, P.* and *Neumann, A. W.*: Adv. Colloid Interf. Sci. *39* (1992) 347.
183. *Prokop, R. M., Jyoti, A., Eslamian, M., Garg, A., Mihaila, M., del Río, O. I., Susnar, S. S., Policova, Z.* and *Neumann, A. W.*: Colloids Surfaces A: Physicochem. Eng. Aspects *131* (1998) 231.
184. *Lu, J. J., Yu, L. M. Y., Cheung, W. W. Y., Policova, Z., Li, D., Hair, M. L.* and *Neumann, A. W.*: Colloids Surfaces B: Biointerfaces *29* (2003) 119.
185. *Yu, L. M. Y., Lu, J. J., Chiu, I. W. Y., Leung, K. S., Chan, Y. W., Zhang, L., Policova, Z., Hair, M.* and *Neumann, A. W.*: Colloids and Surface B: Biointerfaces *36* (2004) 167.
186. *Lu, J. Y., Distefano, J., Philips, K., Chen, P.* and *Neumann, A. W.*: Respir. Physiol. *115* (1999) 55.
187. *Lu, J. J., Cheung, W. W. Y., Yu, L. M. Y., Policova, Z., Li, D., Hair, M. L.* and *Neumann, A. W.*: Respir. Physiol. Neurobiol. *130* (2002) 169.
188. *Lu, J. J., Yu, L. M. Y., Cheung, W. W. Y., Goldthrope, I. A., Zuo, Y. Y., Policova, Z., Cox, P. N.* and *Neumann, A. W.*: Colloids Surfaces B: Biointerfaces *41* (2005) 145.
189. *Zuo, Y. Y., Li, D., Acosta, E., Cox, P. N* and *Neumann A. W.*: Langmuir *21* (2005) 281.
190. *Wüstneck, R., Wüstneck, N., Vollhardt, D., Miller, R.* and *Pison, U.*: Mater. Sci. Eng. C *8–9* (1999) 57.
191. *Yu, L. M. Y., Lu, J. J., Chan, Y. W., Ng, A., Zhang, L., Hoorfar, M., Policova, Z., Grundke, K.* and *Neumann, A. W.*: J. Appl. Physiol. *97* (2004) 704.
192. *Cheng, P.* and *Neumann, A. W.*: Colloids Surf. *62* (1992) 297.
193. *Pratt, W. K.*: Digital Image Processing: PIKS Inside, 3rd edn (2001) Wiley, New York.
194. *Gonzalez, R. C.* and *Woods, R. E.*: Digital Image Processing, 2nd edn (2002) Upper Saddle River, Prentice Hall, New York.
195. *Seul, M., O'Gorman, L.* and *Sammom, M. J.*: Practical Algorithms for Image Analysis, Description, Examples, and Code (1999) Cambridge university press, New York.
196. *Qiu, P.* and *Bhandarkar, S. M.*: Pattern recognition letters *17* (1996) 849.
197. *Canny, J.*: IEEE Trans. Pattern Anal. Mach. Intell. *8* (1986) 679.
198. *Shen, J.* and *Castan, S.*: CVGIP: Graphical Models and Understanding *54* (1992) 112.
199. *Boie, R. A., Cox, I.* and *Rehak, P.*: Proceedings of the IEEE Conference on Computer Vision and Pattern Recognition (1986) 100.
200. *Boie R. A.* and *Cox, I.*: Proceedings of the IEEE First International Conference on Computer Vision (1987) 450.
201. *Kimura, T., Taguchi, A.* and *Murata, Y.*: Electronics and Communications in Japan *83* (2000) 61.
202. *Wong, H. S., Caelli T.* and *Guan, L.*: Pattern Recognition *33* (2000) 427.
203. *Hou, Z. J.* and *Wei, G. W.*: Pattern Recognition *35* (2002) 1559.
204. *Heath, M. D., Sarkar, S., Sanocki, T.* and *Bowyer, K.W.*: IEEE Trans. Pattern Anal. Mach. Intell. *19* (1997) 1338.
205. *Heath, M. D., Sarkar, S., Sanocki, T.* and *Bowyer, K. W.*: Computer Vision and Image Understanding *69* (1998) 38.
206. *Nguyen, T. B.* and *Ziou, D.*: Pattern Recognition Letters *21* (2000) 805.
207. *Parker, J. R.*: Algorithms for Image Processing and Computer Vision (1997) John Wiley & Sons, New York.
208. *Jasper, J. J.*: J. of Phys. Chem. Ref. Data *1* (1972) 841.
209. *Vargaftik, N. B., Volkov, B. N.* and *Voljak., L. D.*: J. Phys. Chem. Ref. Data *12* (1983) 817.
210. *Prokop, R. M., Jyoti, A., Cox, P., Frndova, H., Policova, Z.* and *Neumann, A. W.*: Colloids Surfaces B: Biointerfaces *13* (1999) 117.
211. *Kobayashi, T., Shido, A., Nitta, K., Inui, S., Ganzuka, M.* and *Robertson, B.*: Respir. Physiol. *80* (1990) 181.
212. *Davies, J. T.* and *Rideal, E. K.*: Interfacial Phenomena, 2nd edn (1963) Academic Press, New York.
213. *Notter, R. H., Taubold, R.* and *Mavis, R. D.*: Exp. Lung Res. *3* (1982) 109.
214. *Dargaville, P. A.* and *Morley, C. J.*: Acta Paediatr. *89* (2000) 1397.
215. *Taeusch, H. W., Lu, K. W., Goerke, J.* and *Clements, J. A.*: Am. J. Respir. Crit. Care Med. *159* (1999) 1391.
216. *McCormack, F. X.*: Chest. *111* (1997) 114 S.
217. *Yu, S. H., McCormack, F. X., Voelker, D. R.* and *Possmayer, F.*: J. Lipid Res. *40* (1999) 920.
218. *Tashiro, K., Kobayashi, T.* and *Robertson, B.*: Acta Paediatr. *89* (2000) 1439.
219. *Kobayashi, T., Ohta, K., Tashiro, K., Nishizuka, K., Chen, W. M., Ohmura, S.* and *Yamamoto, K.*: J. Appl. Physiol. *86* (1999) 1778.
220. *Lu, K. W., Taeusch, H. W., Robertson, B., Goerke, J.* and *Clements, J. A.*: Am. J. Respir. Crit. Care Med. *162* (2000) 623.
221. *Lu, K. W., Taeusch, H. W., Robertson, B., Goerke, J.* and *Clements, J. A.*: Am. J. Respir. Crit. Care Med. *164* (2001) 1531.
222. *Taeusch, H. W.* and *Keough, K. M. W.*: Pediatric Pathology and Molecular Medicine *20* (2001) 519.
223. *Harris, J. M.*: in: Harris, J. M. (Ed) Poly(ethylene glycol) Chemistry: Biotechnical and Biomedical Applications (1992) Plenum Press, New York, pp. 1.
224. *Zalipshy, S.* and *Harris, J. M.*: in: Harris, J.M. and Zalipshy, S. (Eds), Poly(ethylene glycol) Chemistry and Biological Applications (1997) American Chemical Society, Washington DC, pp. 1.
225. *Brackenbury, A. M., Malloy, J. L., McCaig, L. A., Yao, L. J., Veldhuizen, R. A. W.* and *Lewis, J. F.*: Eur. Respir. J. *19* (2002) 41.
226. *Holmberg, K., Jönssm, B., Kronbeg, B.* and *Lindman, B.*: Surfactants and Polymers in Aqueous Solution, 2nd edn (2003) Wiley, New York.
227. *Hiemenz, P. C.* and *Rajagopalan, R.*: Principles of Colloid and Surface Chemistry, 3rd edn (1997) Marcel Dekker, New York.
228. *Kuhl, T., Guo, Y., Alderfer, J. L., Berman, A. D., Leckband, D., Israelachvili, J.* and *Hui, S. W.*: Langmuir *12* (1996) 3003.
229. *Meyuhas, D., Nir, S.* and *Lichtenberg, D.*: Biophys. J. *71* (1996) 2602.
230. *Gennes, Pierre-Gilles de*: Scaling Concepts in Polymer Physics (1979) Cornell University Press, Ithaca.
231. *Zuo, Y. Y.*: Ph.D. Thesis, University of Toronto, in preparation.
232. *Zuo, Y. Y., Lu, J. J., Hoorfar, M., Zhang, L., Policova, Z., Li, D.* and *Neumann, A. W.*: 77th ACS Colloids and Surfaces Symposium, Atlanta, GA, June 15–18, 2003.
233. *Gitiafroz, R., Policova, Z., Hoorfar, M., Lu, J. J.* and *Neumann, A. W.*: 78th ACS Colloids and Surfaces Symposium, New Haven, CT, Jun 20–23, 2004.
234. *Zuo, Y. Y., Gitiafroz, R., Acosta, E., Policova, Z., Cox, P. N., Hair, M. L.* and *Neumann, A. W.*: Biophys. J. (Submitted).

Received: 01. 02. 2005
Accepted: 14. 04. 2005

Correspondence to

Dr. A. Wilhelm Neumann
Department of Mechanical and Industrial Engineering
University of Toronto
5 King's College Road, Toronto, ON, Canada, M5S 3G8
Tel.: 1-4 16-9 78-12 70
Fax: 1-4 16-9 78-77 53
E-mail: neumann@mie.utoronto.ca

The authors of this paper

Yi Y. Zuo received his M.Sc. from University of Science and Technology Beijing in 2001. He is currently pursuing his Ph.D. with Dr. A. W. Neumann in the Department of Mechanical and Industrial Engineering, University of Toronto. His research interest is in the surface tension measurements of lung surfactant systems, interfacial transport phenomena, and advanced image analysis for measuring the interfacial properties of biofluids.

Dr. A. W. Neumann received his Dr. Rer. Nat in Chemical Physics at University of Mainz, Germany in 1962, his habilitation in Physical Chemistry of Surfaces, at University of Stuttgart, Germany, in 1972. He is currently a professor emeritus at the Department of Mechanical and Industrial Engineering, University of Toronto. His main research interests include: 1) fundamental surface thermodynamic studies from both experimental and theoretical points of view, e. g. contact angle interpretation and surface energetics; 2) development of novel methodologies in applied surface thermodynamics, e. g. application of image analysis and computer-aided techniques in measurements of surface thermodynamic properties such as surface tension, contact angle, and line tension; 3) applications of surface thermodynamics to the process of biomedical relevance, e. g. energetic characterization of biosurfaces, and most recently the study of lung surfactant.